the plant journal

SEB SOCIETY FOR EXPERIMENTAL BIOLOGY

The Plant Journal (2023) **113,** 833–850 doi: 10.1111/tpj.16088

Arabidopsis immune responses triggered by cellulose- and mixed-linked glucan-derived oligosaccharides require a group of leucine-rich repeat malectin receptor kinases

Marina Martín-Dacal[1,2,†], Patricia Fernández-Calvo[1,2,*,†], Pedro Jiménez-Sandoval[3], Gemma López[1], María Garrido-Arandía[1,2], Diego Rebaque[1,2,‡], Irene del Hierro[1], Diego José Berlanga[1,2], Miguel Ángel Torres[1,2], Varun Kumar[1], Hugo Mélida[1,§], Luis F. Pacios[1,2], Julia Santiago[3] and Antonio Molina[1,2,*]

[1]*Centro de Biotecnología y Genómica de Plantas, Universidad Politécnica de Madrid (UPM) – Instituto Nacional de Investigación y Tecnología Agraria y Alimentaria (INIA/CSIC), Campus de Montegancedo UPM, 28223, Pozuelo de Alarcón, Spain,*

[2]*Departamento de Biotecnología-Biología Vegetal, Escuela Técnica Superior de Ingeniería Agronómica, Alimentaría y de Biosistemas, UPM, 28040, Madrid, Spain,*

[3]*University of Lausanne (UNIL), Biophore Building, Département de Biologie Moléculaire Végétale (DBMV), UNIL Sorge, CH-1015, Lausanne, Switzerland*

Received 28 October 2022; revised 15 December 2022; accepted 21 December 2022; published online 29 December 2022.
*For correspondence (e-mail patricia.fernandez.calvo@upm.es; antonio.molina@upm.es).
†These authors contributed equally to this work.
‡Present address: Division of Glycoscience, School of Biotechnology, Royal Institute of Technology (KTH), Stockholm, Sweden
§Present address: Área de Fisiología Vegetal, Departamento de Ingeniería y Ciencias Agrarias, Universidad de León, León, Spain

SUMMARY

The plant immune system perceives a diversity of carbohydrate ligands from plant and microbial cell walls through the extracellular ectodomains (ECDs) of pattern recognition receptors (PRRs), which activate pattern-triggered immunity (PTI). Among these ligands are oligosaccharides derived from mixed-linked β-1,3/β-1,4-glucans (MLGs; e.g. β-1,4-D-$(Glc)_2$-β-1,3-D-Glc, MLG43) and cellulose (e.g. β-1,4-D-$(Glc)_3$, CEL3). The mechanisms behind carbohydrate perception in plants are poorly characterized except for fungal chitin oligosaccharides (e.g. β-1,4-D-$(GlcNAc)_6$, CHI6), which involve several receptor kinase proteins (RKs) with LysM-ECDs. Here, we describe the isolation and characterization of *Arabidopsis thaliana* mutants impaired in glycan perception (*igp*) that are defective in PTI activation mediated by MLG43 and CEL3, but not by CHI6. *igp1*–*igp4* are altered in three RKs – AT1G56145 (IGP1), AT1G56130 (IGP2/IGP3) and AT1G56140 (IGP4) – with leucine-rich-repeat (LRR) and malectin (MAL) domains in their ECDs. *igp1* harbors point mutation E906K and *igp2* and *igp3* harbor point mutation G773E in their kinase domains, whereas *igp4* is a T-DNA insertional loss-of-function mutant. Notably, isothermal titration calorimetry (ITC) assays with purified ECD-RKs of IGP1 and IGP3 showed that IGP1 binds with high affinity to CEL3 (with dissociation constant K_D = 1.19 ± 0.03 μM) and cellopentaose (K_D = 1.40 ± 0.01 μM), but not to MLG43, supporting its function as a plant PRR for cellulose-derived oligosaccharides. Our data suggest that these LRR-MAL RKs are components of a recognition mechanism for both cellulose- and MLG-derived oligosaccharide perception and downstream PTI activation in Arabidopsis.

Keywords: *Arabidopsis thaliana*, cellulose, mixed-linked glucans (MLGs), immunity, oligosaccharides, pattern recognition receptors (PRRs), leucine-reach repeat/Malectin receptor kinase (LRR-MAL RK).

INTRODUCTION

Plants have evolved a complex immune system that comprises several defense layers and mechanisms for the recognition of pathogens and pests that cooperatively interact to restrict plant infection. One of these layers, known as pattern-triggered immunity (PTI), is based on the recognition of damage- and microbe-associated molecular patterns (DAMPs and MAMPs) derived from plants or microorganisms, respectively, by plasma membrane-resident pattern recognition receptors (PRRs) (Ngou et al., 2022). Upon DAMP/MAMP recognition by ectodomains (ECDs) of PRRs, additional proteins are recruited to form ligand–PRR complexes, triggering the activation of PRR cytoplasmic protein kinase domains (KDs) that initiate phosphorylation and signaling cascades (Boutrot &

Zipfel, 2017; Ngou et al., 2022). Early PTI responses include increases in the cytoplasmic concentration of the second messenger, Ca^{2+}, the production of reactive oxygen species (ROS) by NADPH oxidases (e.g. respiratory burst oxidase homolog protein D, RBOHD), the phosphorylation of mitogen-activated protein kinases (MAPKs) and Ca^{2+}-dependent protein kinases (CPKs), and transcriptional reprogramming that ultimately restrict the colonization of the plant by pathogens or pests (Bigeard et al., 2015; Boutrot & Zipfel, 2017). DAMPs or MAMPs are molecules with different biochemical composition, such as peptides, carbohydrates (oligosaccharides) or fatty acids, among other molecules (Bigeard et al., 2015; Boutrot & Zipfel, 2017; Ngou et al., 2022).

Many PRR/peptidic DAMP/MAMP pairs triggering PTI responses have been elucidated, like AtPep1 DAMP and bacterial flg22 MAMP peptides, which are directly bound by Arabidopsis PEPR1/2 and FLS2 PRRs, respectively (Bigeard et al., 2015; Boutrot & Zipfel, 2017; Tang & Wang, 2017). These PRRs require members of the SOMATIC EMBRYOGENESIS RECEPTOR KINASE (SERK) family, like BAK1, for active complex formation and downstream PTI activation (Bigeard et al., 2015; Boutrot & Zipfel, 2017; Tang & Wang, 2017). FLS2 and PEPR1/2 are receptor kinase (RK) proteins with an ECD harboring leucine-rich repeats (LRRs), a transmembrane domain (TM) and a cytoplasmic serine/threonine KD. Plant PRRs with LRR-ECDs comprise about 50% of RKs (Bellande et al., 2017; del Hierro et al., 2021). The *Arabidopsis thaliana* genome has more than 600 genes encoding members of RKs, receptor-like proteins (RLPs, with ECD and TM but lacking the KD) and receptor proteins (RPs, with ECD but lacking TM), which in some cases are clustered in the same plant genomic region, illustrating their recent evolutionary divergence (del Hierro et al., 2021; Franck et al., 2018; Ngou et al., 2022).

In contrast to the extended knowledge of peptidic DAMP and MAMP perception, our understanding of plant immunity activation by carbohydrate-based DAMPs and MAMPs is scarce. However, carbohydrates are highly abundant molecules in plant and microbial extracellular layers, such as cell walls, and several of them are known to be perceived by the plant immune system and to trigger PTI: oligosaccharides from chitin, e.g. chitohexaose (β-1,4-D-*N*-acetylglucosamine)$_6$ (CHI6), and β-1,3-glucan of fungal/oomycete cell walls, peptidoglycan from bacterial walls, and oligosaccharides derived from plant cell wall polymers, such as cellulose (β-1,4-glucan), mixed-linked glucans (MLGs; β-1,4/β-1,3-glucans), xyloglucan, mannan, xylan and homogalacturonan/pectins (oligogalacturonides or OGs), and from other glycans, such as fructans (Aziz et al., 2007; Claverie et al., 2018; Denoux et al., 2008; Gust et al., 2007; Kaku et al., 2006; Klarzynski et al., 2000; Mélida et al., 2018; Mélida et al., 2020; Versluys et al., 2022; Voxeur et al., 2019; Wanke et al., 2020; Zang et al., 2019). Remarkably, about 50% of RK/RLP/RP from plant genomes have ECDs that are predicted to bind carbohydrate-based ligands and are grouped in different families: lysin motif (LysM), lectins (G-, L- and C-lectins), crinkly-like (CR4L), wall-associated kinases (WAKs), cysteine-rich kinases (CRK/DUF26) and families with malectin (MAL) or malectin-like domains (MLDs) in their ECDs (LRR-MAL, MLD-LRRs and *Catharanthus roseus* receptor-like kinases 1-like, CrRLK1Ls) (Bacete et al., 2018; Bellande et al., 2017; del Hierro et al., 2021). Therefore, oligosaccharide–PRR pairs are expected to play a role in immune activation by carbohydrates in plants (Cosgrove, 2022; Wan et al., 2021).

Cellulose, a linear polymer of β-1,4-glucosyl residues, is present in all plants, most algae, some protists and microbial (bacteria and oomycete) extracellular matrixes or walls, being the most abundant biomolecule on earth (Burton & Fincher, 2009; Kloareg et al., 2021; Morgan et al., 2013). MLGs, consisting of unbranched and unsubstituted chains of β-1,4-glucosyl residues interspersed by β-1,3-linkages, are widely distributed as matrix polysaccharides in the cell walls of plants from the Poaceae family (cereals), but have also been reported in *Equisetum* spp. and other vascular plants (Fry et al., 2008; Sørensen et al., 2008), bryophytes and algae (Popper & Fry, 2003; Salmeán et al., 2017), bacteria (Pérez-Mendoza et al., 2015), and fungi and oomycetes (Fontaine et al., 2000; Pettolino et al., 2009; Rebaque et al., 2021). MLG-derived oligosaccharides, e.g. MLG43 (β-1,4-D-(Glc)$_2$-β-1,3-D-Glc), MLG443 (β-1,4-D-(Glc)$_3$-β-1,3-D-Glc) and MLG34 (β-1,3-D-Glc-β-1,4-D-Glc$_2$), are perceived with different degrees of specificity by the immune system of several plant species, e.g. Arabidopsis, *Capsicum annuum* (pepper), *Hordeum vulgare* (barley), *Oryza sativa* (rice), and *Solanum lycopersicum* (tomato), with MLG43-mediated PTI responses being the best characterized (Barghahn et al., 2021; Rebaque et al., 2021; Yang, Liu, et al., 2021a; Yang, Liu, et al., 2021b). Similarly, cellulose-derived oligosaccharides, e.g. β-1,4-D-(Glc)$_2$ to β-1,4-D-(Glc)$_6$ (cellobiose to cellohexaose or CEL2–CEL6), trigger PTI responses in Arabidopsis, rice and other plant species (Klarzynski et al., 2000; Locci et al., 2019; Rebaque et al., 2021; Souza et al., 2017; Yang, Liu, et al., 2021a; Yang, Liu, et al., 2021b). MLG- and CEL-derived oligosaccharides are self-alert signals (DAMPs) of plant colonization by pathogens, as they can be released from plant cell walls by the activity of microbial endoglucanases, such as cellulases, secreted during plant colonization (Gámez-Arjona et al., 2022; Yang, Liu, et al., 2021b). MLGs can also be perceived as MAMPs by plant species that do not contain them in their cell walls (Barghahn et al., 2021; Rebaque et al., 2021).

The mechanisms of oligosaccharide perception by the mammal immune system through carbohydrate

recognition domains are well documented (Bacete et al., 2018; Cummings et al., 2022; Taylor et al., 2022). In contrast, our understanding of the structural basis of oligosaccharide perception by plant PRRs is limited and mainly restricted to PRRs of the LysM family, e.g. CHITIN ELICITOR RECEPTOR KINASE 1 (CERK1) and LysM motif receptor kinases 4 and 5 (LYK4 and LYK5). Such proteins harbor promiscuous ECDs involved in the activation of PTI mediated by structural diverse ligands, such as CHI6–CHI8, β-1,3-glucan (laminarihexaose, LAM6) and MLGs (MLG43, MLG34 and MLG443) (Cao et al., 2014; Desaki et al., 2018; Liu et al., 2012; Mélida et al., 2018; Miya et al., 2007; Rebaque et al., 2021; Wanke et al., 2020; Willmann et al., 2011; Yang, Liu, et al., 2021b). Immune responses triggered by CHI6, LAM6 and MLG43 are partially impaired in *cerk1* single and *lyk4 lyk5* double mutants (Cao et al., 2014; Liu et al., 2012; Mélida et al., 2018; Rebaque et al., 2021; Shimizu et al., 2010; Yang et al., 2022). However, a direct binding of LAM6 and MLG43 to the *A. thaliana* CERK1 ECD was discarded based on *in silico* structural molecular dynamics simulations and isothermal titration calorimetry (ITC) binding assays (del Hierro et al., 2021). These data suggest that CERK1, LYK4 and LYK5 might function as protein partners in the LAM6 perception system. Notably, rice OsCERK1 seems to be the PPR binding MLG43 and MLG443, whereas OsCeBIP, the rice chitin PRR, is required for the perception of these ligands, but not for their direct binding (Yang, Liu, et al., 2021b). In addition to LysM-PRRs, Arabidopsis WAK receptors (e.g. WAK1 and WAK2) are PRRs required for the perception of OGs, and the CrRLK1L member FERONIA (FER), with two malectin-like domains in its ECD, binds homogalacturonans (Brutus et al., 2010; Tang et al., 2022). Recently, two LRR-RKs have been implicated in PTI activation triggered by CEL-derived oligosaccharides in Arabidopsis (Zarattini et al., 2021), and the CELLO-OLIGOMER RECEPTOR KINASE 1 (CORK1, an LRR-MAL RK) has been described to be required for CEL3 perception and PTI activation in Arabidopsis (Tseng et al., 2022). However, the structural bases of CEL-derived oligosaccharide recognition by these putative PRRs have not yet been elucidated.

We designed genetic screenings in Arabidopsis to identify mutants impaired in glycan (e.g. MLGs) perception (*igp*). We selected several mutants (*igp1*–*igp9*) that are impaired in the perception of both MLG43 and CEL3, but not CHI6. Here we show that *IGP1*, *IGP2/IGP3* and *IGP4* encode three RK members (AT1G56145/CORK1, AT1G56130 and AT1G56140, respectively) with LRR-MAL in their ECDs. We also demonstrate that the ECD of IGP1, previously described as CORK1 (Tseng et al., 2022), binds directly to CEL3 and CEL5 with high affinity, further supporting its function as a plant PRR involved in the perception of cellulose-derived oligosaccharides. These results expand our knowledge of the mechanisms of immune activation by oligosaccharides in plants.

RESULTS

Identification and isolation of Arabidopsis *igp1*–*igp9* mutants

We generated an ethyl methanesulfonate (EMS) mutagenized population of the *A. thaliana* aequorin-based Ca^{2+} sensor line Col-0^{AEQ} (Knight et al., 1991; Mélida et al., 2018; Ranf et al., 2011) to perform a genetic screening aiming to isolate mutants impaired in glycan perception (*igp*; Figure S1). First, we performed a genetic screening to identify *igp* mutants impaired in MLG perception, and we selected for the screening MLG43 trisaccharide as its PTI-mediated responses in Arabidopsis are the best characterized (Barghahn et al., 2021; Rebaque et al., 2021; Yang, Liu, et al., 2021a; Yang, Liu, et al., 2021b). Eight-day-old seedlings (about 6400 individuals) of 13 M_2 EMS-mutagenized Col-0^{AEQ} families were grown in microtiter plates together with the Col-0^{AEQ} control line, treated with 100 μM MLG43, and changes of cytoplasmic Ca^{2+} concentration were then determined in a luminometer (Figure S1). Several mutants (*igp1*^{AEQ}–*igp9*^{AEQ}) that showed a weaker Ca^{2+} burst than that of Col-0^{AEQ} plants were selected for further genetic characterization (backcrosses and allelism tests; Figures 1a and S2; Table S1). To assess the specificity of MLG43 perception impairment in *igp* mutants we also treated *igp* lines with CHI6 (50 μM) and found that it triggered similar Ca^{2+} bursts in the *igp* mutants as those observed in Col-0^{AEQ} plants, whereas *cerk1*^{AEQ} plants were fully impaired in CHI6 perception, as previously reported (Figures 1b and S2; Mélida et al., 2018; Rebaque et al., 2021). These data suggest that the mechanism of perception of CHI6 and MLG43 in Arabidopsis might not be identical, in contrast to what has been described in rice (Yang et al., 2022). No mutations were found in the *Aequorin* gene sequence in *igp1*^{AEQ}–*igp3*^{AEQ} (Online data set), and no differences were observed in endogenous Ca^{2+} levels between the *igp1*^{AEQ}–*igp3*^{AEQ} and Col-0^{AEQ} seedlings, based on Ca^{2+} discharge analyses (Figure S1). These data support that the lower Ca^{2+} bursts observed in MLG43-treated *igp1*^{AEQ}–*igp3*^{AEQ} seedlings were the result of the defective perception of MLG43.

igp1^{AEQ}, *igp2*^{AEQ} and *igp3*^{AEQ} mutants harbor recessive mutations (chi-square test, $0.7 > P > 0.5$, $0.5 > P > 0.3$ and $0.8 > P > 0.7$, respectively; Table S2), and *igp2*^{AEQ} and *igp3*^{AEQ} were allelic (chi-square test, $P > 0.95$; Figure S1; Table S1). Genomic DNA from F_2 progeny of *igp1*^{AEQ}, *igp2*^{AEQ} and *igp3*^{AEQ} backcrosses with Col-0^{AEQ} was sequenced and assembled to identify putative mutations (frequency higher than 0.99 in alignments; Table S2). We found that *igp1*^{AEQ} has a point mutation in the *AT1G56145* gene, encoding an RK with

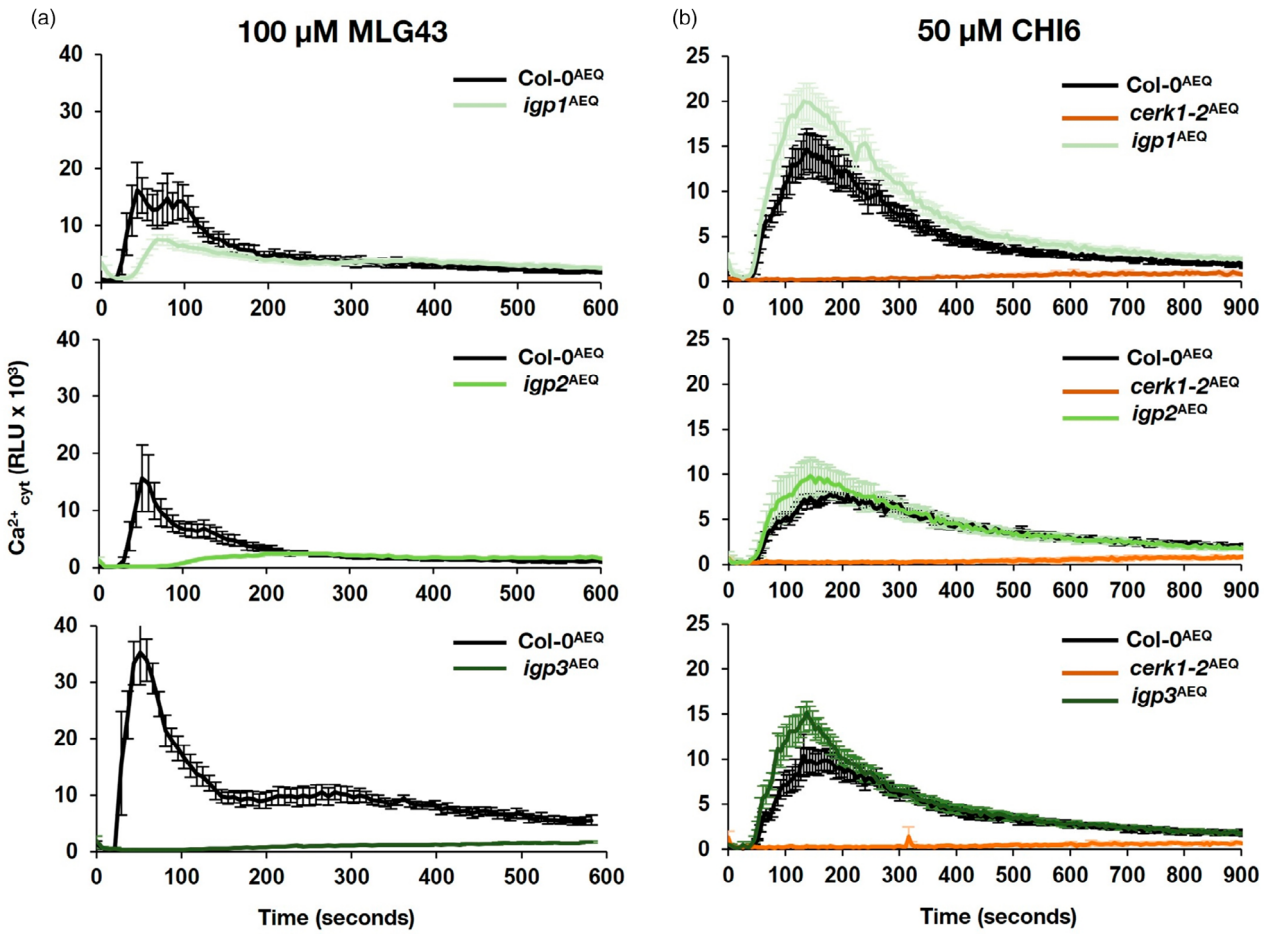

Figure 1. Identification of *Arabidopsis thaliana* mutants impaired in glycan perception (*igp*).
Ca^{2+} burst upon application of (a) 100 µM MLG43 and (b) 50 µM CHI6 was measured as relative luminescence units (RLUs) over time in Col-0^{AEQ} and *igp*^{AEQ} mutants. The *cerk1-2*^{AEQ} line, impaired in CHI6 perception, was included for comparison. Data represent the mean ± standard error ($n = 4$ in Col-0^{AEQ} and *cerk1-2*^{AEQ}; $n = 8$ in *igp*^{AEQ}). Data are from one of the four experiments performed that gave similar results.

an LRR-MAL ECD, which resulted in E906K amino acid change in its KD (Figure 2a). On the other hand, *igp2*^{AEQ} and *igp3*^{AEQ} share the same point mutation in the *AT1G56130* gene, encoding an additional LRR-MAL RK, which resulted in G773E amino acid change in its KD (Figure 2a). Notably, these two LRR-MAL RKs are in a genomic cluster with two additional genes, *AT1G56120* and *AT1G56140*, which encode two additional LRR-MAL RKs (Yang, Wang, et al., 2021). These RKs are members of a specific group of LRR-MAL proteins that comprise at least 13 genes in the *A. thaliana* genome, with *AT1G56120*, *AT1G56130*, *AT1G56140* and *AT1G56145* genes constituting a specific clade of the family (Figure S3; del Hierro et al., 2021). This family has a few characterized members, such as *RFK1* (*AT1G29720*), that promote compatible pollen grain hydration and pollen tube growth (Lee & Goring, 2021), the recently described IGP1/CORK1 protein (Tseng, et al., 2022), and the so-called BRASSINOSTEROID (BR) KINASE (BSK) 3-INTERACTING RLK (BSR) members, which are not well characterized (Yang, Wang, et al., 2021).

Using reverse transcription quantitative real-time polymerase chain reaction (RT-qPCR), we determined that the expression of *AT1G56140*, but not that of *AT1G56120*, *AT1G56130* and *AT1G56145*, was upregulated upon treatment of seedlings with MLG43, CHI6 and other glucans (e.g. CEL3; Figure S3). We then selected T-DNA insertional mutants of *AT1G56120* and *AT1G56140* genes and tested their perception of MLG43 and CHI6 by determining the upregulation of PTI marker genes *WRKY53* and *CYP81F2* using RT-qPCR (Mélida et al., 2018, Rebaque et al., 2021; Figure S3). The expression of these genes was compromised in the *at1g56140* knockout mutant, whereas the expression in the *at1g56120* mutant was very similar to that of Col-0 (Figure S3). Both mutants displayed a similar upregulation of *WRKY53* and *CYP81F2* expression to that of wild-type plants upon CHI6 treatment (Figure S3). To further validate the phenotype of the *at1g56140* mutant,

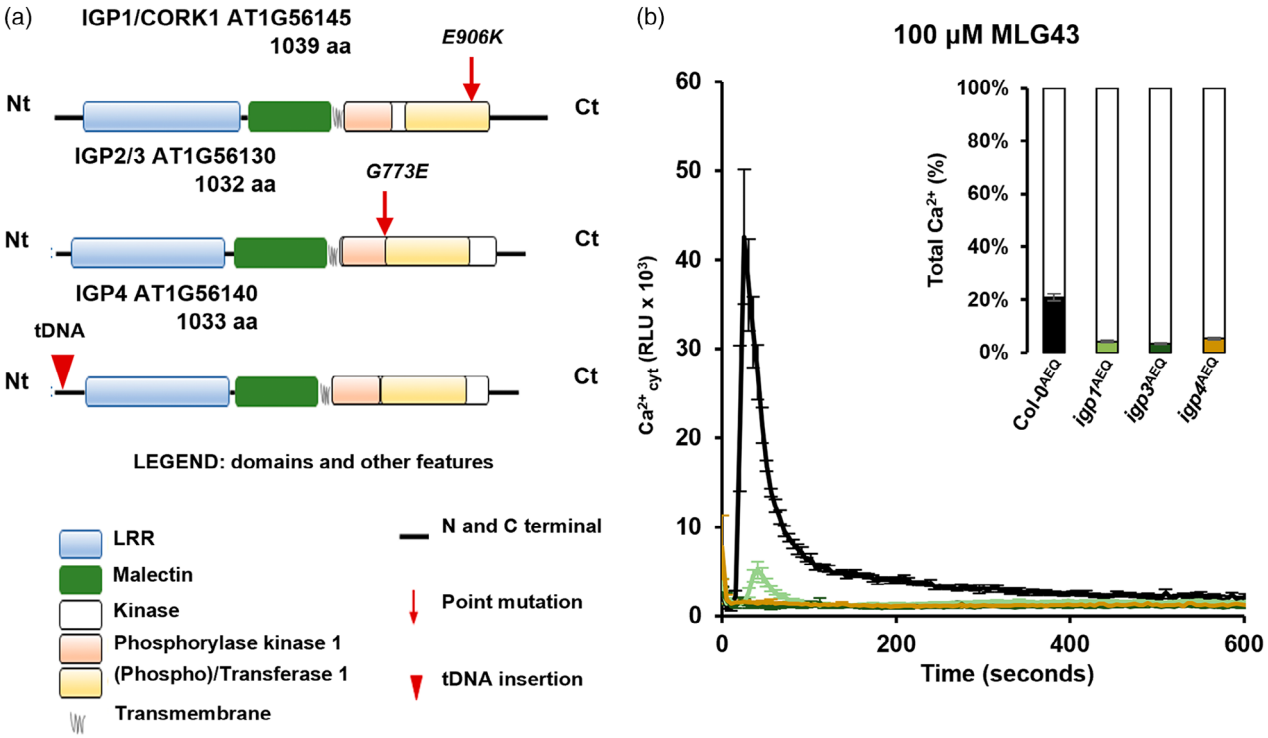

Figure 2. Identification of mutations in *igp1–igp4* mutants.
(a) Representation of IGP1, IGP2/3 and IGP4 domains: leucine-rich repeat (LRR; blue), malectin (MAL; green), phosphorylase kinase (orange) and phophotransferase (yellow) of kinase domain (KD; white), N- and C-terminal domains (black lines) and transmembrane domain (TM; gray). Red arrows indicate the position of the mutations in the coding regions of *igp1*^{AEQ}, *igp2*^{AEQ} and *igp3*^{AEQ}, and the red triangle indicates the insertion of the T-DNA sequence in *igp4* (Online data set). (b) Ca^{2+} burst measured as relative luminescence units (RLUs) over time in Col-0^{AEQ}, *igp1*^{AEQ}, *igp3*^{AEQ} and *igp4*/*at1g56140*^{AEQ} seedlings upon treatment with 100 µM MLG43. Data represent the mean ± standard error ($n = 4$ in Col-0^{AEQ} and $n = 8$ in *igp*^{AEQ}). Total Ca^{2+} was discharged by the addition of 1 mM $CaCl_2$ to the wells and these values were used for the calculation of the total Ca^{2+} % induced by MLG43 treatment (graph at top right). This is one of three experiments performed that gave similar results.

we crossed this line with Col-0^{AEQ} and the homozygous *at1g56140*^{AEQ} line generated was tested for Ca^{2+} burst upon MLG43 and CHI6 treatment. *at1g56140*^{AEQ} was impaired in MLG43 but not CHI6 perception, like *igp1*^{AEQ}–*igp3*^{AEQ}, and this defective response was not caused by any alteration in the endogenous levels of Ca^{2+}, as revealed by Ca^{2+} discharge experiments. Accordingly, the *at1g56140* mutant was named *igp4* and selected for further analyses to determine the contribution of AT1G56140/IGP4 RK in the regulation of PTI responses mediated by MLG- and CEL-derived oligosaccharides (Figure 2b). We assessed the impact of the *igp1–igp4* mutations on plant developmental phenotypes and no significant differences were observed in the rosette and silique size and morphology of *igp1*^{AEQ} and *igp4*^{AEQ} plants in comparison with Col-0^{AEQ} or *cerk1-2*^{AEQ}, whereas *igp2*^{AEQ}/*igp3*^{AEQ} plants have rosettes and siliques slightly smaller than those of Col-0 plants or *cerk1-2*^{AEQ} (Figure S4). As the last two mutants are allelic, we stuck to *igp3*^{AEQ} to characterize its function across this article. Accordingly, we will refer to *IGP3* and IGP3, when discussing the gene and the encoded protein, respectively, affected in this mutant.

LRR-MAL RKs are also required for the perception of additional cellulose- and MLG-derived oligosaccharides

To assess the specificity of MAMPs and DAMPs that activate the Ca^{2+} response through these LRR-MAL RKs, we measured the Ca^{2+} bursts in *igp1*^{AEQ}, *igp3*^{AEQ}, *igp4*^{AEQ} and Col-0^{AEQ} seedlings after treatment with different DAMPs, i.e. carbohydrate ligands such as CEL3 and OGs (DP10–DP12) and the peptide AtPep1, and the MAMP flg22. Remarkably, the three *igp*^{AEQ} lines were almost fully impaired in CEL3-mediated Ca^{2+} burst activation, suggesting that these RKs are also required for the perception of cellulose-derived oligosaccharides (Figure 3a,b). In contrast, the Ca^{2+} responses induced by flg22, OGs and AtPep1 treatments in the mutants were similar to those observed in Col-0^{AEQ} (Figure 3c–e). The response of *igp5*^{AEQ}–*igp9*^{AEQ} mutants to CEL3 was also impaired (Figure S5), further supporting the hypothesis that the mechanisms of perception of MLG43 and CEL3 in Arabidopsis share some components. As additional cellulose- and MLG-derived oligosaccharides, such as cellobiose (CEL2), cellotetraose (CEL4), cellopentaose (CEL5) and MLG34, trigger PTI in Arabidopsis (Locci

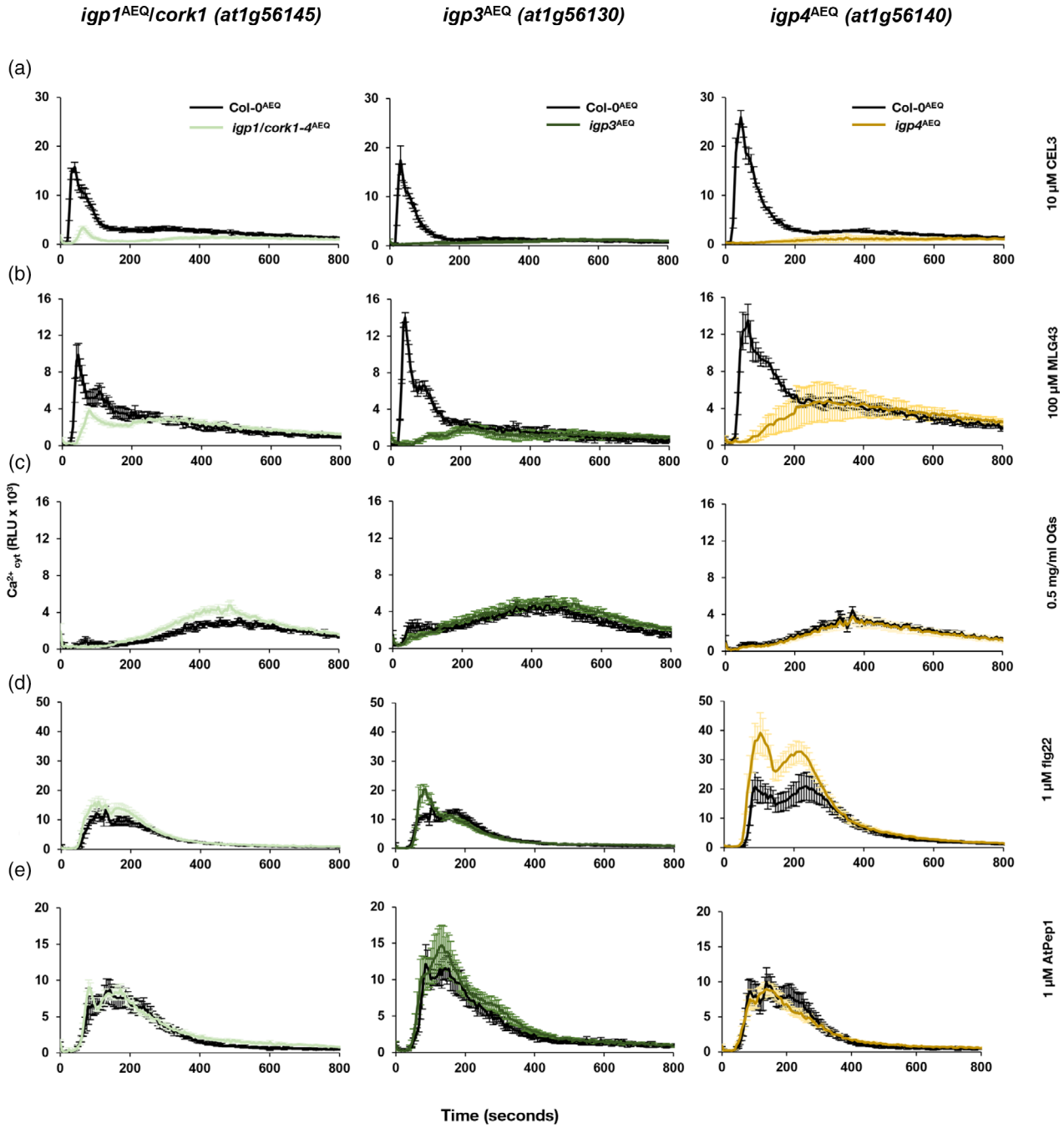

Figure 3. Cytoplasmic calcium burst triggered by CEL3 is impaired in *igp*^{AEQ} mutants.
Ca^{2+} burst measured as relative luminescence units (RLUs) over time in Col-0^{AEQ}, *igp1*^{AEQ}, *igp3*^{AEQ} and *igp4*^{AEQ} seedlings after treatment with: (a) 10 µM CEL3; (b) 100 µM MLG43; (c) 0.5 mg mL^{-1} OGs; (d) 1 µM flg22; and (e) 1 µM AtPep1. Data represent the mean ± standard error (n = 4 in Col-0^{AEQ} and n = 8 in *igp*^{AEQ}). Data are from one of three experiments performed that gave similar results.

et al., 2019; Rebaque et al., 2021; Souza et al., 2017), we also determined the Ca^{2+} burst activated by these glycans in *igp*^{AEQ} mutants and Col-0^{AEQ}. The three mutants showed reduced Ca^{2+} influxes in comparison with Col-0^{AEQ} upon treatment with MLG34, CEL4 and CEL5 (Figure 4b,d,e), indicating that the three LRR-MAL RKs are required for the perception of these cellulose- and MLG-derived oligosaccharides. By contrast, the Ca^{2+} influxes triggered by CEL2 were, under our experimental conditions, very low, even in Col-0^{AEQ} (Figure 4f), suggesting that this disaccharide has low immunogenic activity in Arabidopsis, and that CEL3 is the cellulose-derived oligosaccharide with the lowest degree of poyimerization (DP) perceived through the sensing mechanism involving these RKs (Figure 4c).

To further validate whether the mechanism of perception of cellulose- and MLG-derived oligosaccharides in Arabidopsis share some PRRs and signaling components, we performed cross-elicitation experiments by treating 8-day-old Col-0^{AEQ} seedlings, first with MLG43 or CEL3, and a few minutes later with either CEL3 or MLG43. In Col-0^{AEQ} seedlings first treated with MLG43, Ca^{2+} influxes were not observed upon the second application of CEL3 (MLG43 + CEL3), similarly to what was observed after treatments with CEL3 + CEL3 and MLG43 + MLG43 (Figure S6), indicating that the mechanisms of perception of MLG43 and CEL3 share molecular components in Arabidopsis.

To confirm the role of this group of LRR-MAL receptors as potential RKs for cellulose- and MLG-derived oligosaccharide perception and PTI activation, we first monitored ROS production in *igp1*^{AEQ}, *igp3*^{AEQ}, *igp4*, Col-0 and *rbohD* lines, impaired in DAMP/MAMP-triggered ROS production (Morales et al., 2016), upon treatment with MLG43, CEL3 and CHI6. The ROS burst was partially impaired in the *igp* mutants compared with the Col-0 plants after treatment with MLG43, and was significantly reduced, even to a higher extent, after CEL3 treatment (Figure 5a,b). In both cases, the reduction in ROS was not as noticeable as in *rbohD*. Notably, the ROS burst in *igp* mutants upon treatment with CHI6 and flg22 was not altered in comparison with Col-0 plants (Figure S7), as observed for the Ca^{2+} burst (Figure 3). Next, we tested the phosphorylation of MAP kinases by Western blot. MPK3 and MPK6 phosphorylation triggered by MLG43 and CEL3 was reduced in *igp1*^{AEQ}, *igp3*^{AEQ} and *igp4* plants, compared with Col-0 plants, whereas it responded similarly to Col-0 in response to CHI6 (Figure 5c). MPK4/11 phosphorylation was almost undetectable in either CEL3-treated or MLG43-treated plants, as reported previously (Rebaque et al., 2021). Last, we performed RT-qPCR analysis to study the expression of two PTI-marker genes upregulated by CHI6 and MLG43 (*WRKY53* and *CYP81F2*; Mélida et al., 2018, Rebaque et al., 2021). The upregulation of *WRKY53* and *CYP81F2* in response to MLG43 and CEL3 was partially impaired in *igp1*^{AEQ}, *igp3*^{AEQ} and *igp4* seedlings, compared with Col-0 plants, whereas it was similar in response to CHI6 (Figure 5d,e). Together, these data support the role of the three LRR-MAL RKs in the perception of cellulose-derived oligosaccharides and, to a lesser extent, in the perception of MLG-derived oligosaccharides.

As previous works reported that MLG perception in Arabidopsis and rice involved LysM-PRRs (e.g. CERK1, LYK4 and LYK5 in Arabidopsis; Rebaque et al., 2021, Yang, Liu, et al., 2021a), we determined ROS production, MPK3/MPK6 phosphorylation and PTI marker upregulation upon treatment with MLG43 or CEL3 in seedlings of Col-0, *cerk1-2* and the *cerk1-2 lyk4 lyk5* triple mutant, which was generated in this work (Figure S8). *cerk1-2* and *cerk1-2 lyk4 lyk5* plants displayed similar ROS kinetics and bursts to those of Col-0 after CEL3 treatment, and only a minor diminution upon MLG43 treatment in comparison to Col-0, whereas this PTI response was greatly impaired after CHI6 treatment (Figure S8). Moreover, a slight reduction of the phosphorylation of MPK3/MPK6 in these mutants, compared with Col-0, was observed upon MLG43 and CEL3 treatment, although it was weaker than that observed with CHI6 (Figure S8). Also, the MLG43-mediated upregulation of *WRKY53* and *CYP81F2* was only partially affected in *cerk1-2* and *cerk1-2 lyk4 lyk5* plants, whereas it was not altered upon CEL3 treatment (Figure S8). These data indicate that MLG43 perception may involve CERK1, LYK4 and LYK5 LysM RKs, as described previously for MLGs in Arabidopsis and rice (Rebaque et al., 2021; Yang, Liu, et al., 2021b), whereas these RKs have almost no contribution to CEL3 perception.

Model structures of IGP1, IGP3 and IPG4 proteins point to their function as RKs

Malectin (MAL) domains like those present in the ECDs of the LRR-MAL RK family have been previously described in animals to bind short glycans, based on the NMR structure of MAL from *Xenopus laevis* in complexes with maltose and nigerose (Schallus et al., 2010). The MAL domain and MLD are present in at least three families of plant RKs (LRR-MAL, MLD-LRRs and CrRLK1Ls; Yang, Wang, et al., 2021), and the ECDs of several CrRLK1L members, e.g. ANXUR1 (ANX1), ANX2 and FERONIA (FER), have been crystallized, but no oligosaccharide ligands were identified in ITC binding experiments (Moussu et al., 2018; Xiao et al., 2019). Phylogenetic analyses of MAL domains of *A. thaliana* LRR-MAL RK members (represented by IGP1/CORK1 and AT1G56145) revealed that the MAL domain is highly conserved in cruciferous and other dicot species (Figure S9; Yang, Wang, et al., 2021). On the other hand, the MAL domain of IGP1/CORK1, IGP3 and IGP4 are evolutionarily divergent from ANX1 and ANX2 and *Xenopus* sp. MLD domains (Figure S9; Yang, Wang, et al., 2021).

The model structures of IGP1/CORK1, IGP3 and IGP4 in the AlphaFold database display a spatial arrangement of all domains that does not properly describe the expected organization of these LRR-MAL RKs (Figure S10). Therefore, to explore the impact of *igp1* and *igp2*/*igp3* point mutations in the KD of these RKs, we first obtained models with the correct domain organization, as described in the Experimental procedures. These models provide a complete picture of the proteins to be used as initial geometries for further computational studies (Figure S11). We then used TM-ALIGN (Zhang & Skolnick, 2005) to evaluate the structural similarity of MAL domains from IGP1/CORK1, IGP3 and IGP4 with several entries in the Protein Data Bank (PDB, https://www.rcsb.org) with MAL and MLD domains (five plant RKs from CrRLK1Ls and nine human and

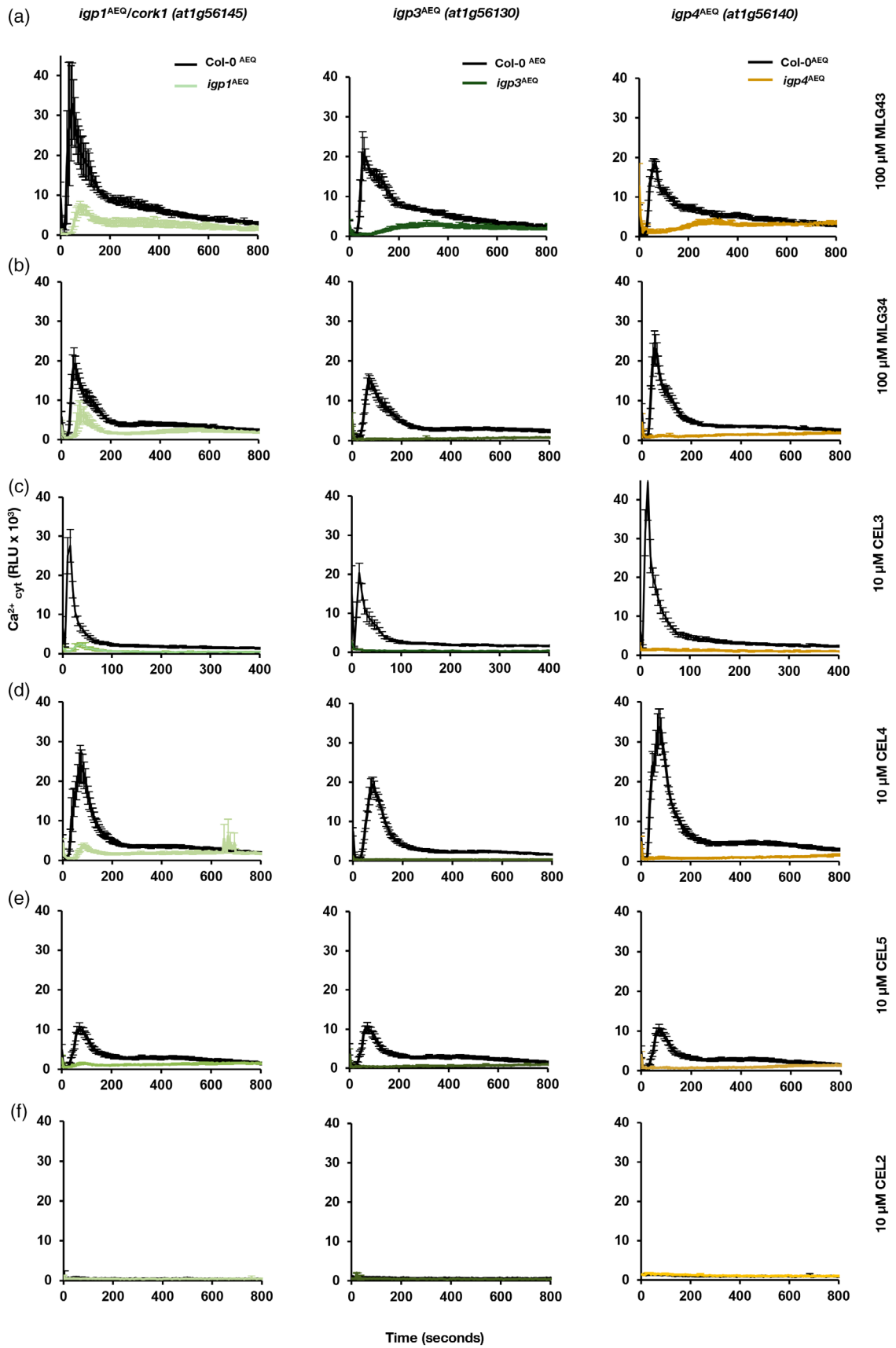

Figure 4. Calcium burst in response to MLG34- and cellulose-derived oligosaccharides is impaired in *igp* mutants.
Ca^{2+} burst measured as relative luminescence units (RLUs) over time in 8-day-old Col-0^{AEQ}, *igp1*^{AEQ}, *igp3*^{AEQ} and *igp4*^{AEQ} seedlings after treatment with: (a) 100 μM MLG43; (b) 100 μM MLG34; (c) 10 μM CEL3; (d) 10 μM CEL4; (e) 10 μM CEL5; and (f) 10 μM CEL2. Data represent the mean ± standard error ($n = 3$ in the case of Col-0 ^{AEQ} and $n = 12$ in the case of *igp*^{AEQ}). The *x*-axis scale in (c) has been shortened for a better comparison of the enhanced response of seedlings to CEL3. Data are from one of three experiments performed that gave similar results.

bacteria proteins), including the NMR structures of malectin from *Xenopus laevis* in complex with maltose (Schallus et al., 2010), an apo form and a complex with nigerose (Schallus et al., 2008), and the crystal structure of tandem MLDs from the ANX1/ANX2 ECDs (Moussu et al., 2018). In all cases, TM scores between 0.623 and 0.710 were found, thus indicating highly similar folds of IGP MAL domains to animal malectin and to plant MLD structures.

Similar structural comparison analyses were performed for the KDs of IGP1/CORK1, IGP3 and IGP4, with some kinase crystals, like MPK6 from Arabidopsis (5CI6, Wang et al., 2016; 6DTL, Putarjunan et al., 2019). The structural alignment data showed that the IGP1/CORK1 KD is noticeably different from that of the two other RKs because of the extra loop seen in the intracellular part of its complete structure (indicated by an arrow in Figure S11), which is not predictable from IGP protein sequence alignments. Notwithstanding, the conformation of side chains of catalytic residues was found to be identical in wild-type and mutant structures, a result worth emphasizing as the mutation positions are near the catalytic site in both IGP1/CORK1 and IGP3 (Figure S11). Next, we tested *in silico* the possible structural impact of the single mutations of E906K in IGP1/CORK1 and G773E in IGP2/IGP3 KDs by generating new model structures of the KD of wild-type and mutants with AlphaFold 2. We found that the backbones remained unaltered, and that E906K in IGP1 and G773E in IGP2/IGP3 had the effect of increasing the surface patch associated with the mutated position (Figure S11). However, the major effect of these single mutations was found in the surface electrostatic potential (Figure S11). The region around E906 in wild-type IGP1/CORK1 shows a weakly negative electrostatic character, whereas in the *igp1* mutant the E906 negative charge of IGP1/CORK1 is substituted for a K906 positive charge, which gives rise to a strongly positive electrostatic potential in a large area around position 906 (Figure S11). The equivalent region around G773 in wild-type IGP2/IGP3 displays a weakly positive electrostatic character, which becomes strongly negative upon the G773E mutation (Figure S11). It is noted that these electrostatic effects extend over a surface region far larger than that expected from the small, exposed surface areas of residues 906 and 773 (Figure S11). These changes in the KD domains of IGP1/CORK1 and IGP2/IGP3 LRR-MAL RKs might explain their loss of functionality. Additional mutations in the KD of IGP1/CORK1 have been proven recently to impair its kinase activity in phosphorylation experiments performed *in vitro* with CORK1 recombinant proteins (wild-type and mutant versions) expressed in *Escherichia coli* (Tseng, et al., 2022).

The ECD of IGP1/CORK1 directly binds cellulose-derived oligosaccharides CEL3 and CEL5

Based on the initial structural models of MAL domains in the three LRR-MAL RKs and their similarities with the MAL domain from *Xenopus* sp. that binds short glycans (Figure S11; Schallus et al., 2010), we tested whether ECDs of these LRR-MAL RKs could be glycan receptors for cellulose- and MLG-derived oligosaccharides. We expressed the ECDs of IGP1/CORK1, IGP3 and IGP4 in insect cells and purified them by affinity chromatography. As the ECD of IGP3 turned out to form aggregates, this ECD was not suitable for further purification steps and was not available for binding experiments (Figure S12). Then, ITC experiments (Sandoval & Santiago, 2020) were carried out to test the binding of MLG43 and CEL3 to IGP1/CORK1 and IGP4 ECDs. The ITC results proved the existence of direct interactions between CEL3 and the ECD of IGP1/CORK1 (K_D = 1.19 ± 0.03 μM; Figure 6a), but not with the ECD of IGP4 (Figure S12). However, the results obtained with ITC clearly indicated that these ECDs did not bind, at least directly, to MLG43 (Figures 6a,b and S12). Similar binding experiments were performed with CEL5 and the ECD of IGP1/CORK1 to determine the specificity of receptor–ligand recognition, and direct binding was also detected with similar high affinity (K_D = 1.40 ± 0.01 μM; Figure 6a). The binding reactions measured for CEL3 and CEL5 were exothermic, with a single binding site ($n = 1$) and very similar values of ΔH, indicating that extra sugar subunits in the CEL5 oligomer do not improve the detected binding. These data support the role of the ectodomain of IGP1/CORK1 as a receptor for cellulose-derived oligosaccharides and suggest that IGP4 RK might function as an RK required for the sensing complex for cellulose- and MLG-derived oligosaccharides.

DISCUSSION

Plant immunity is activated by a diverse set of ligands (DAMPs and MAMPs) with different biochemical composition and structure. These DAMPs and MAMPs are specifically perceived by diverse sets of ECDs from plant PRRs, triggering the formation of a ligand–PRR complex that involves additional proteins that contribute to the functionality of the recognition complex (Bigeard et al., 2015; Boutrot & Zipfel, 2017; Ngou et al., 2022). Some of the best-characterized DAMPs and MAMPs are oligoglycans from

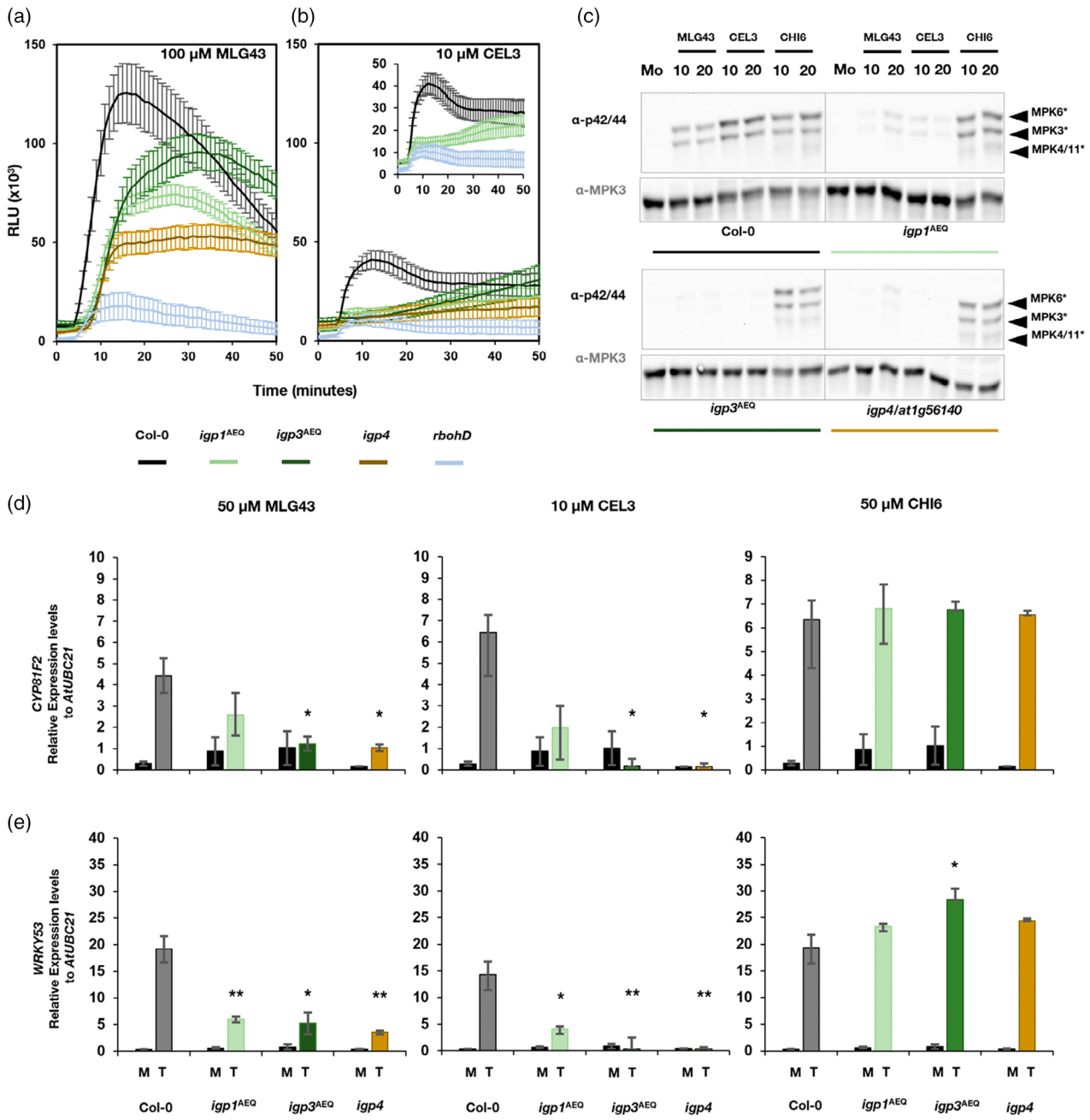

Figure 5. Activation of pattern-triggered immunity (PTI) hallmarks by MLG43, CEL3 and CHI6 in *igp*^{AEQ}.
(a, b) Reactive oxygen species (ROS) production was monitored as H_2O_2 production over a period of 50 min by luminol assays and measured as relative luminescence units (RLUs) in the indicated genotypes; 100 µM MLG43 (a) and 10 µM CEL3 (b) were added 5 min after the transfer to the luminometer of the plate with seedling and luminol reagents. Data represent mean ± standard error ($n = 8$). Comparison with Col-0 assessed by Student's *t*-test ($n = 24$) at the time of the Col-0 peak shows statistically significant differences for *igp1*^{AEQ} and *igp3*^{AEQ} ($P < 0.01$) and *igp4*^{AEQ} ($P < 0.001$) in response to MLG43. Likewise, all three mutants show statistical differences at $P < 0.001$, compared with Col-0, in response to CEL3. *rbohD* plants impaired in ROS production showed statistically significant differences ($P < 0.001$) with both treatments. These results are from one representative experiment out of three performed that gave similar results. The inset in (b) has been included in the graph to allow an easy comparison of the RLU data for *igp1*^{AEQ} and Col-0. (c) Mitogen-activated protein kinase (MAPK) phosphorylation was analyzed in seedlings of Col-0, *igp1*^{AEQ}, *igp3*^{AEQ} and *igp4*^{AEQ} treated with 100 µM MLG43, 10 µM CEL3, 50 µM CHI6 or water (mock). Western blotting using anti-pTEpY antibody (anti-p42/44) for phosphorylated MAPK moieties was performed with samples harvested at 10 and 20 min. Mock samples (Mo) corresponding to a 10-min treatment with water were included as basal expression controls. Black arrows indicate the positions of phosphorylated MPK6 (top), MPK3 (middle) and MPK4/11 (bottom). Anti-MPK3 was used as a total protein control to show the loading of each gel. These results are from one representative experiment out of two performed that gave similar results. (d, e) RT-qPCR analysis in the indicated genotypes. Expression levels of *CYP81F2* (d) and *WRKY53* (e) genes, relative to the housekeeping gene *UBC21* (*AT5G25769*) 30 min after mock treatment (M) or the application of the oligosaccharides (T) are shown. Data represent mean ± standard error of three technical replicates out of three independent biological replicates ($n = 3$). Statistically significant differences between MLG43-, CEL3- or CHI6-treated *igp*^{AEQ} versus treated Col-0 according to Student's *t*-test (*$P < 0.05$, **$0.01 < P > 0.001$, ***$P < 0.001$).

(a)

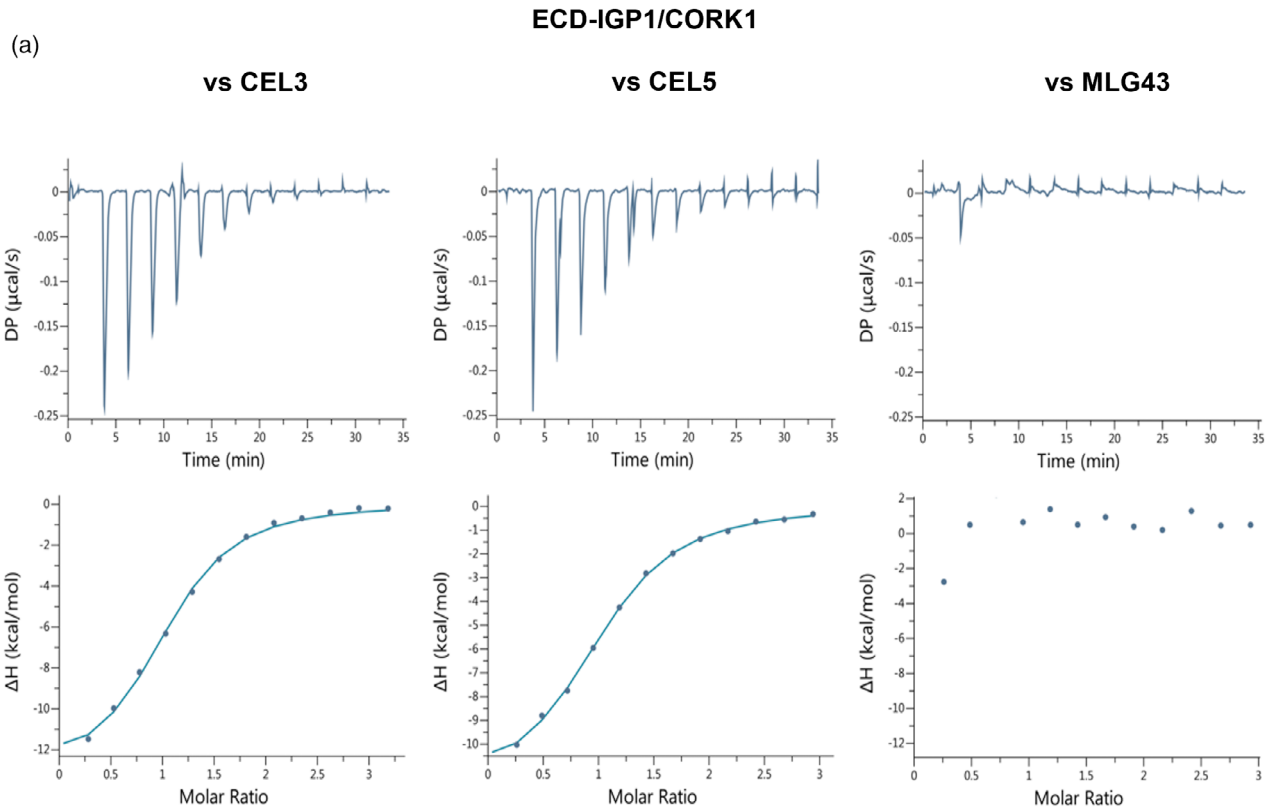

(b)

Ligand (syringe)	Protein (cell)	K_d (µM)	ΔH (kcal/mol)	N
CEL3	AT1G56145 (IGP1/CORK1)	1.19 ± 0.03	13.60 ± 0.30	1
CEL5	AT1G56145 (IGP1/CORK1)	1.40 ± 0.01	12.50 ± 0.15	1
MLG43	AT1G56145 (IGP1/CORK1)	n.d.		
CEL3	AT1G56140 (IGP4)	n.d.		
MLG43	AT1G56140 (IGP4)	n.d.		

Figure 6. The IGP1/CORK1 ectodomain (ECD) directly binds CEL3- and CEL5-derived oligosaccharides.
(a) Isothermal titration calorimetry (ITC) experiments of ECD-IGP1/CORK1 versus CEL3, MLG43 and CEL5. (b) ITC summary of ECD-IGP1 and ECD-IGP4 versus CEL3, MLG43 and CEL5. The binding affinities of ECD-IGP1/CORK1 are reported as K_D (dissociation constant, in micromoles), *DP* indicates measured power differential between the reference and sample cells to maintain a zero temperature between the cells inside the ITC device, *N* indicates the reaction stoichiometry (*N* = 1 for a 1:1 interaction) and Δ*H* indicates the enthalpy variation. Values indicated in the table are means ± SDs of independent experiments (*n* = 2). n.d., no binding detected.

fungal chitin (e.g. CHI6) or plant pectins (e.g. OGs), which are perceived by LysM-PRRs and WAK1/2/FER1-PRRs, respectively (Brutus et al., 2010; Miya et al., 2007; Tang et al., 2022). Several glycan ligands derived from cell walls or extracellular matrixes from plants or microorganisms that trigger immune responses in plants have recently been described (Aziz et al., 2007; Barghahn et al., 2021; Claverie et al., 2018; Denoux et al., 2008; Gust et al., 2007; Kaku et al., 2006; Klarzynski et al., 2000; Mélida et al., 2018; Mélida et al., 2020; Rebaque et al., 2021; Versluys et al., 2022; Voxeur et al., 2019; Wanke et al., 2020; Yang, Liu, et al., 2021a; Yang, Liu, et al., 2021b; Zang et al., 2019). Among them are oligosaccharides derived from β-glucans of plant cell walls, like MLGs (e.g. MLG43, MLG34 and MLG443), or cellulose (e.g. CEL2, CEL3, CEL4, CEL5 and CEL6). Here, we describe a group of *Arabidopsis thaliana* RKs – IGP1, IGP3 and IGP4 – with LRR-MAL domains in their ECDs that are required to trigger immune responses mediated by oligosaccharides derived from cellulose (e.g. CEL3–CEL5) and MLGs (e.g. MLG43 and MLG34) (Figures 1 and 2).

We demonstrate by ITC binding experiments that the IGP1/CORK1 RK is a PRR for cellulose-derived oligosaccharides, further supporting its recently proposed function by Tseng et al. (2022) that identified CORK1/IGP1 in a similar genetic screening to the one performed here. We demonstrate the direct interaction of IGP1/CORK1-ECD with CEL3 and with CEL5 with high affinity (K_D = 1.19 ± 0.03 μM and K_D = 1.40 ± 0.01 μM, respectively), and the absence of binding with MLG43, at least under the *in vitro* conditions of ITC tested (Figures 6 and S12). Our data suggest that the IGP1/CORK1 RK might be a true PRR receptor for CEL3–CEL5 oligosaccharides, and that IGP3 and IGP4 RKs might function in Arabidopsis as components of the PRR complex involved in the perception of these oligosaccharides or the signaling complex activating downstream PTI responses (Figure 5). A recent article reports that two LRR RKs, SIF2 (AT1G51850) and SIF4 (AT1G51820), are also required for the immune responses triggered by cellulose-derived oligosaccharides and could also be part of the PRR complex involved in their perception (Zarattini et al., 2021). Also, a poly(A)-specific ribonuclease (AtPARN, AT1G55870) was found to be required for the regulation of the immune responses triggered by CEL3 in Arabidopsis, probably through a mechanism of degradation of the polyA tail from specific mRNAs (Johnson et al., 2018). However, this AtPARN regulatory mechanism of CEL3-mediated responses acts downstream of CEL3 perception by PRRs at the cell surface described here.

Our results point to the LRR-MAL RK family as a set of plant proteins involved in the perception of carbohydrate-based DAMPs and MAMPs, as previously suggested (del Hierro et al., 2021). So far, the plant RKs described to be involved in glycan perception belong to the LysM, WAK and CrRLK1 RK families (Bellande et al., 2017; Brutus et al., 2010; Cao et al., 2014; del Hierro et al., 2021; Liu et al., 2012; Liu et al., 2016; Tang et al., 2022; Wong et al., 2020). The function of most of these proteins in oligosaccharide perception and PTI activation was discovered through the isolation and characterization of Arabidopsis mutants (e.g. *cerk1*, *lyk4*, *lyk5*, *wak1*, *wak2* and *fer1*). In general, such mutants share redundant functions with additional RKs, and therefore individually they are either unaffected or only partially impaired in PTI responses triggered by specific DAMPs and MAMPs. Accordingly, higher-order RK mutants that overcome redundancy must be analyzed to observe PTI-deficient phenotypes (Brutus et al., 2010; Cao et al., 2014; Dünser et al., 2019; Guo et al., 2018; Liu et al., 2012; Liu et al., 2016; Miya et al., 2007). Similarly, our genetic screening led to the identification of nine mutants impaired in glycan perception (*igp1*–*igp9*), among them *IGP1/CORK1*, *IGP2/IGP3* and *IGP4* have been isolated as mutants impaired in MLG43 recognition, and later proven to also be defective in the perception of cellulose-derived oligosaccharides (CEL3–CEL5; Figures 3 and 4). These results suggest that the mechanisms of perception of CEL- and MLG-derived oligosaccharides overlap in Arabidopsis, and this is supported by CEL3/MLG43 cross-elicitation experiments (Figure S6). However, despite the similarities between the mechanisms of perception of MLG- and CEL-derived oligosaccharides, some differences might exist among them. For example, we found that LysM RKs (i.e. CERK1, LYK4 and LYK5) have a partial contribution in the perception of MLG43 (Figure S8), as described previously (Rebaque et al., 2021). In contrast, their role in CEL3 perception is residual as only minor differences in PTI activation were observed in *cerk1-2* and *cerk1-2 lyk4 lyk5* triple mutants in comparison with Col-0 plants treated with CEL3 (Figure S8). The partial requirement of LysM RKs for MLG perception in Arabidopsis is in line with the described function of rice LysM RK members in the perception of MLG-derived oligosaccharides and immune activation. OsCERK1 has been suggested to be the PRR receptor of MLG-derived oligosaccharides based on microscale thermophoresis analysis performed with the ECD produced in baculovirus, whereas OsCeBiP, the rice receptor for chitin-derived oligosaccharides, has been proposed to be the MLG co-receptor of CERK1, based on the lack of binding of its ECD to these MLG ligands (Yang, Liu, et al., 2021b). The K_D values of ECD–OsCERK1 for MLG43 are in the range of 1–2 μM, similar to that found for IGP1/CORK1 binding to CEL3/CEL5 in this work (Figure 6), and to that of ECD–OsCeBiP for CHI6 (Yang, Liu, et al., 2021b). Of note, the perception of CHI6 is neither altered in *igp1-igp4* nor altered in *igp5-igp9* mutants (Figures 1 and S2), further indicating that Arabidopsis IGP1–IGP9 proteins are not required for CHI6 perception. These data point to separate mechanisms for the perception of CHI6 and the CEL3- and MLG43-derived oligosaccharides in Arabidopsis, but also to some differences in the mechanism of perception of CEL3 (independent of CERK1, LYK4 and LYK5, and with IGP1/CORK1 as a true PRR) and MLG43 (requiring CERK1, LYK4 and LYK5, with the true PRR yet to be determined). The role of LysM RKs in the mechanisms of perception of several glycans and in plant–microbe interactions is an emerging issue (Yang, Wang, et al., 2021). The mechanisms of PTI activation mediated by IGP1, IGP3 and IGP4 LRR-MAL RKs described here also differ from that of pectin and OG perception involving FER1 and WAK1–WAK2 (Brutus et al., 2010; Dünser et al., 2019; Tang et al., 2022), respectively, and that of other MAMPs and DAMPs (e.g. flg22 and AtPEP1), because the Ca^{2+} burst in *igp1*^{AEQ}–*igp4*^{AEQ} upon treatment with these elicitors was similar to that of Col-0^{AEQ} plants (Figure 3c–e). All these data support the specific function of IGP1/CORK1, IGP3 and IGP4 RKs in MLG- and CEL-derived oligosaccharide recognition.

The crystallized structures of ECDs of CERK1- and chitin-derived oligosaccharides revealed the structural

basis of this recognition (Liu et al., 2012; Yang, Liu, et al., 2021b). Other plant ECD-RKs like ANX1, ANX2 and FER1, which harbor two tandem MLDs, have been also purified and crystallized, but their putative glycoligand(s) has not been identified (Moussu et al., 2018). Notably, the MLDs of ANX1, ANX2 and FER1 seem to show some differences compared with those MAL domains present in the ECDs of the three IGP RKs identified in this work, which also contain an N-terminal LRR domain (Figure S11; (Yang et al., 2021)). We have generated *de novo* structural models for the three LRR-MAL RKs, and these models suggest that IGP1/CORK1, IGP3 and IGP4 have similar structures, in line with their putative recent evolutionary divergence (Figure S3), although IGP1/CORK1 has an extra loop in its KD (Figure S11). Remarkably, MAL domains of these RKs are structurally very similar to that of the MAL protein of *Xenopus* sp., which is involved in oligosaccharide binding, and to that of plant ANX1/ANX2 from the CrRLK1 family (Figure S11). In recent reports by Tseng et al. (2022), two Phe residues conserved in all *A. thaliana* MAL domains, but not in MAL from *Xenopus* sp. (Schallus et al., 2010) are noted as essential for CEL3 perception and PTI activation, but this hypothesis has not been validated through binding experiments. Therefore, we hypothesize that the LRR domain of ECDs in IGP1/CORK1 might be essential for the formation of the structural pocket involved in the observed CEL3 and CEL5 binding. Obtaining crystallized structures of CEL3/ECD-IGP1 will contribute to decipher the structural bases of CEL3–CEL5 recognition by LRR-MAL ECD.

We show here that *igp1* and *igp2/igp3* mutants have point mutations in their KDs that may impact their functionality (Figure 2). E906K in IGP1/CORK1 and G773E in IGP3 do not seem to impair the catalytic sites of these RKs, which are predicted to be almost identical to that of wild-type KDs (Figure S11). However, such mutations are predicted to increase the surface patch, resulting in drastic changes on the surface electrostatic potential of the residues around the mutated positions (Figure S11). As kinase activity can be altered by mutations at distant residues from the active site (McClendon et al., 2014), we can hypothesize that E906K and G773E mutations might either affect the catalytic activity of the KDs or interfere with the interaction of the RK KDs with other RKs, like true PRR for MLG43 perception, co-receptors proteins of IGP1/CORK1 PRR (e.g. IGP2/3 and IGP4) or additional protein partners.

The exogenous application of glycans enhanced disease resistance of different plant species to diverse pathogens, acknowledging the relevance of these carbohydrate-based ligands released during plant–microbe interaction in the regulation of plant disease resistance (Mélida et al., 2018; Rebaque et al., 2021). This oligosaccharide-mediated priming effect on PTI and disease resistance has driven the development of sustainable crop protection solutions based on combinations of active glycans (DAMPs and MAMPs; Chaliha et al., 2020, Lemke et al., 2022). The discovery of counterpart receptors for these active glycans in crops would accelerate the selection of the corresponding genes in breeding programs to enhance crop disease resistance. Notably, the *IGP1/CORK1*, *IGP3* and *IGP4* genes are in a cluster in the *A. thaliana* genome, indicating recent duplication events (Yang, Wang, et al., 2021). These genes form part of a family of at least 13 members that has not been characterized in detail previously, except for RFK1, a protein involved in pollen tube growth (Lee & Goring, 2021). This clade of LRR-MAL RKs seems to be conserved and diversified in dicots (Fig. S10) and in some monocots, like rice. However, the few relatives RKs found in grasses are structurally dissimilar and phylogenetically distant (Yang, Wang, et al., 2021).

The MLG- and cellulose-derived oligosaccharides can also be released upon alteration of plant cell wall integrity triggered by other stresses (e.g. salt or drought) or across plant development (e.g. during cell wall remodeling; Bacete et al., 2022, Gigli-Bisceglia et al., 2022). During these processes plant endogenous enzymes can hydrolase cell wall polysaccharides, as described recently for a *Zea mays* (maize) GH17 licheninase that releases MLG43-derived and other oligosaccharides (Kraemer et al., 2021). The characterization of the role of glycan-mediated responses in these additional processes must be determined to understand their interaction with PTI/disease resistance responses and their impact on plant fitness. Also, the regulation of the homeostasis of cell wall-derived oligosaccharides needs to be analyzed in depth. For example, several plant berberine-bridge enzymes control CEL–oligosaccharide homeostasis by oxidating the anomeric carbon of CEL3–CEL6 oligosaccharides, thus reducing both their activity as DAMPs and their preferred use as a carbon source by fungi (Benedetti et al., 2018). In summary, our results contribute to further understanding the mechanisms of perception of oligosaccharides by the plant immune system and to expand the set of families of PRRs and the ECD structures involved in ligand recognition and immune activation in plants.

EXPERIMANTAL PROCEDURES

Biological material and growth conditions

The *A. thaliana* lines used in this study, all in the Columbia-0 (Col-0) background, were Col-0^{AEQ}, carrying the calcium reporter aequorin protein (Knight et al., 1991; Ranf et al., 2011), *cerk1-2*^{AEQ} (Ranf et al., 2011), *rbohD* (Morales et al., 2016) and *igp*^{AEQ}, isolated in this work. The *cerk1-2 lyk4 lyk5* triple mutant was generated by crossing *cerk1-2* and the *lyk4 lyk5* double mutant (Rebaque et al., 2021) and selecting the triple mutants with the oligonucleotides described (Table S3). The *at1g56140* (*igp4*) and the *at1g56120* T-DNA mutants were obtained from NASC (SALK_005808 and SALK_043782, respectively). Plants used for cytoplasmatic Ca^{2+} measurements and ROS were grown in 96-well plates (with one seedling per well), and

for MAPK phosphorylation and gene expression analyses plants were grown in 24-well plates (with approx. 10 seedlings per well). Seedlings were grown under long-day conditions (14 hours of light) at 19–22°C in half-strength liquid MS medium. Plants were also grown in a soil–vermiculite (3:1) mixture under a short-day photoperiod (10 h of light/14 h of dark, 21–20°C) or a long-day photoperiod (14 h of light/10 h of dark, 19–22°C).

Carbohydrates used in the experiments

MLG43 (β-1,4-D-$(Glc)_2$-β-1,3-D-Glc; #O-BGTRIB), MLG34 (β-1,3-D-$(Glc)_2$-β-1,4-D-Glc; #O-BGTRIA), hexaacetyl-chitohexaose (CHI6; β-1,4-D-$(GlcNAc)_6$; #O-CHI6), CEL3 (β-1,4-D-$(Glc)_3$; O-CTR), CEL4 (β-1,4-D-$(Glc)_4$; #O-CTE), CEL5 (β-1,4-D-$(Glc)_5$; #O-CPE) were purchased from Megazyme (https://www.megazyme.com). CEL2 (cellobiose, β-1,4-D-$(Glc)_2$; C7252) came from Sigma-Aldrich (https://www.sigmaaldrich.com). OGs (galacturonan oligosaccharides mixture DP10/DP15; GalAα1–4(GalAα1–4)8_{-13}GalA; GAT114) were from ELICITYL (https://www.elicityl-oligotech.com). Peptides flg22 and AtPEP1 were from EZBiolab (http://www.ezbiolab.com) and Abyntek (https://www.abyntek.com), respectively.

Genetic screening to identify *igp* mutants

Col-0^{AEQ} seeds were mutagenized with 0.3% EMS for 17 h. Seeds were sown in soil–vermiculite (3:1) to obtain next-generation seeds (e.g. M_1 and M_2) (Ranf et al., 2012). M_2 seedlings were grown *in vitro* for 8 days, and cytoplasmic Ca^{2+} influxes were evaluated using a Varioskan Lux Reader luminometer (ThermoFisher Scientific, https://www.thermofisher.com) upon treatment with 100 μM MLG43, as described (Rebaque et al., 2021). Seedlings with low response to MLG43 were transferred to soil (230 putative mutants out of 6400 total seedlings screened), self-crossed and then the Ca^{2+} burst was tested in F_1 seedlings to confirm the impaired response to MLG43. Validated *igp* mutants (*igp1*^{AEQ}–*igp3*^{AEQ} and *igp5*^{AEQ}–*igp9*^{AEQ}, described here, and *igp10*^{AEQ}–*igp20*^{AEQ}, not described here) were selected for further characterization and backcrossed with Col-0^{AEQ}. Total Ca^{2+} discharge was performed by treating seedlings with 1 M $CaCl_2$ and then the Ca^{2+} burst was measured in the luminometer.

Mapping by whole-genome sequencing and SNP analysis

Tissue from 50 individuals of F_2 *igp*^{AEQ} × Col-0^{AEQ} segregating plants with impaired response to MLG43 and from control line Col-0^{AEQ} was harvested and pooled for whole-genome sequencing of gDNA to identify single-nucleotide polymorphisms (SNPs) associated with phenotypes in *igp*^{AEQ}. Sequencing (150-bp paired-end reads) was performed on an Illumina platform (https://www.illumina.com) to reach a coverage of 30 million reads (Andrews, 2010), which were aligned with BWA-MEM 0.7.17 (Macrogen, https://dna.macrogen.com) against the *A. thaliana* TAIR10 genome release (Li, 2013). BAM files were obtained with SAMTOOLS 1.15.1 (http://www.htslib.org). The variant caller 16GT DOCKER IMAGE was employed to obtain VCF files (Danecek et al., 2021; Luo et al., 2017). From these VCF files, chromosome, position, reference, alternate and allelic depth (AD) fields were extracted with BCFTOOLS 1.15.1, and SNPs were subtracted from the resulting files. Frequency was calculated from AD fields as follows: [AD-alternate allele/(AD-alternate allele + AD-reference allele)]. SNPs with frequency values higher than 0.99 were selected for further analyses (Online data set; Table S2).

Determination of PTI responses

Reactive oxygen species (ROS; H_2O_2) production was determined in 10-day-old seedlings after treatment with MAMPs and DAMPs using the luminol assay, as described by Rebaque et al. (2021). MAPK activation was determined in 12-day-old seedlings grown on half-strength liquid MS medium and treated with water (mock) or different oligosaccharides for 0, 10 and 20 mins. Then seedlings were harvested and Western blotting was performed as described previously, with a few modifications (Rebaque et al., 2021). Gene expression analysis was carried out in 12-day-old seedlings grown on half-strength liquid MS medium, and treated with oligosaccharides (i.e. 100 μM MLG43, 10 μM CEL3 or 50 μM CHI6) or water (mock) for 30 min. Then total RNA extraction and RT-qPCR analyses were performed as described by Rebaque et al. (2021). Gene expression and normalization to mock samples were determined using PFAFFL (Pfaffl, 2001). The oligonucleotides used for PCR are described in Table S3.

Phylogenetic analysis

The evolutionary history of IGP proteins was inferred using the minimum evolution (ME) method (Rzhetsky & Nei, 1992). The bootstrap consensus tree inferred from 1000 replicates is taken to represent the evolutionary history of the taxa analyzed (Felsenstein, 1985). Branches corresponding to partitions reproduced in less than 50% bootstrap replicates are collapsed. The percentage of replicate trees in which the associated taxa clustered together in the bootstrap test (1000 replicates) are shown next to the branches (Felsenstein, 1985). The evolutionary distances were computed using the p-distance method (Nei & Kumar, 2000). The ME tree was searched using the close-neighbor-interchange (CNI) algorithm (Nei & Kumar, 2000) at a search level of 1. The neighbor-joining algorithm (Saitou & Nei, 1987) was used to generate the initial tree. The analysis involved 25 amino acid sequences. All ambiguous positions were removed for each sequence pair and a total of 709 positions were present in the final data set. Evolutionary analyses were conducted in MEGA 6 (Tamura et al., 2013).

Structure analyses *in silico*

Model structures of IGP1/CORK1/AT1G56145, IGP3/AT1G56130 and IGP4/AT1G56140 were downloaded from the AlphaFold Protein Structure Database (Tunyasuvunakool & Adler, 2021). They present six identifiable domains: N-terminal containing a signal peptide annotated in PFAM (Mistry et al., 2021), LRR, MAL, TM, KD and the C-terminal tail. The pDDT metric over most of LRR, MAL and KDs is ≥90% (Figure S10) (Jumper et al., 2021). To achieve the proper extracellular/TM/intracellular domain separation, and taking the IGP4 model as the benchmark, we proceeded as follows: (i) torsions were applied to backbone dihedral angles in the segment following MAL (magenta box in Figure S10) with CHIMERA 1.15 (Pettersen et al., 2004); (ii) energy minimization of the extended segment joining the MAL and TM domains was performed with CHIMERA 1.15, keeping all the remaining structure fixed; (iii) the resulting structure was inserted in a pre-equilibrated model of a bilayer composed of 256 phosphatidylcholine (POPC) lipids with a pore of radius 8 Å, downloaded from the CHARMM-GUI archive (Jo et al., 2007), and the protein-bilayer system was parametrized using the CHARMM 3.6 force field (Huang et al., 2017) with CHARMM-GUI (Jo et al., 2008); (iv) the protein bilayer system was solvated with a 16-Å margins solvation box and NaCl 0.150 M salt ions with VMD 1.9.3 (Humphrey et al., 1996), and the whole structure was optimized with 10 000 conjugated gradient minimization steps using NAMD 2.14 (Phillips & Hardy, 2020). The optimized final structure of IGP4 was then used as the input for modeling the corresponding structures of IGP1/CORK1 and IGP3 with SWISS-MODEL (Waterhouse et al., 2018) in 'user template mode'. The structural

comparisons of MAL and KD were analyzed with the TM-Align web server (Zhang & Skolnick, 2005) The structural analysis of mutants IGP1-E906K and IGP3-G773E, and their corresponding wild-type KDs, was addressed by modeling them separately with AlphaFold 2 (Jumper et al., 2021) using ColabFold (Mirdita & Schütze, 2022). Poisson–Boltzmann (PB) electrostatic potentials (EPs) were computed with the Adaptive Poisson Boltzmann Solver, APBS 3.0.0 (Jurrus et al., 2018) through its plug-in in PYMOL 2.5.1 (Schrödinger, 2020), solving the nonlinear PB equation in sequential focusing multigrid mode at 3D grids of $161^3 = 4\,173\,281$ points (approx. 0.5-Å step size), with $T = 298$ K, ionic concentration of 0.150 M (NaCl), and dielectric constants of 4.00 for proteins and 78.54 for water. The PB EP was then mapped onto molecular surfaces computed and rendered with PYMOL 2.5.1 (Schrödinger, 2020).

Protein expression and purification from insect cells

Codon-optimized synthetic genes corresponding to the ectodomains of AT1G56145 (residues 25–630), AT1G56140 (residues 29–636) and AT1G56130 (residues 30–636) from Invitrogen GeneArt were cloned into a modified pFastBac donor vector (Geneva Biotech, https://geneva-biotech.com) harboring the *Drosophila BiP* (Smakowska-Luzan et al., 2018) or the 30K *Bombyx mori* (Soejima et al., 2013) secretion signal peptides, and with a TEV (tobacco etch virus protease) cleavable C-terminal StrepII-9xHis tag. Baculovirus vectors were generated in DH10MultiBac *E. coli* cells (Geneva Biotech). Briefly, virus amplification was carried out in *Spodoptera frugiperda* Sf9 cells (Geneart, Thermo Fisher Scientific) and was used to infect *Trichoplusia ni* Tnao38 cells (Hashimoto et al., 2012) for protein expression. The cells were grown for 1 day at 28°C and for 2 days at 22°C with gentle shaking. The secreted proteins were subjected to tandem affinity purification, using Ni^{2+} (HisTrap excel, equilibrated in 25 mM KPi, pH 7.8, and 500 mM NaCl; GE Healthcare, https://www.gehealthcare.com) and Strep columns (Strep-Tactin Superflow high-capacity; IBA, https://www.iba.de) equilibrated in (25 mM Tris, pH 8.0, 250 mM NaCl, 1 mM EDTA. Affinity tags were removed using His-tagged TEV protease in a 1:50 ratio at 4°C overnight. Separation of cleavage tags and aggregated proteins was performed using size-exclusion chromatography on a Superdex 200 Increase 10/300 GL column (GE Healthcare) equilibrated in 20 mM citric acid, pH 5.0, 150 mM NaCl. Proteins were analyzed for purity and structural integrity by SDS-PAGE.

Analytical size-exclusion (SEC) chromatography

Analytical size-exclusion experiments were performed on a Superdex 200 Increase 10/300 GL column (GE Healthcare) equilibrated in 20 mM citric acid, pH 5.0, 150 mM NaCl. A 400-μg portion of protein (aprox. 6 μM) was injected using a loop of 1 mL, and the sample was eluted with a flow of 0.5 mL min^{-1}. UV absorbance at 280 nm was used to monitor the elution of proteins. The peak fractions were analyzed by SDS-PAGE followed by Coomassie blue staining.

Isothermal titration calorimetry (ITC)

Experiments were performed at 25°C using a MicroCal PEAQ-ITC (Malvern Instruments, https://www.malvernpanalytical.com) with a 200-μL standard cell and a 40-μL titration syringe. Briefly, for ITC experiments in MicroCal PEAQ-ITC, proteins were gel-filtrated into the ITC buffer (20 mM sodium citrate, pH 5.0, 150 mm NaCl). A 3-μL sample of potential ligand (CEL3, CEL5 or MLG43) was injected at a concentration range between 135 and 400 μM into the ITC cell containing ECDs of AT1G56145 or AT1G56140 protein at 9 μM. A total of 13 injections were performed at 150-s intervals with a 500-rpm stirring speed. Dilution heat was corrected using the thermograph of the titration of the ligand into the cell containing only buffer as a control. Experiments were performed in duplicate or triplicate, unless otherwise specified, and data were analyzed using the MICROCAL PEAQ-ITC analysis software provided by the manufacturer. All ITC runs used for data analysis have an *N* ranging from 0.98 to 1.05. The *N* values were fitted to 1 in the analysis.

ACCESSION NUMBERS

Genes described in this work are: *IGP1/AT1G56145*; *IGP2/AT1G56130*; *IGP3/AT1G56130*; *IGP4/AT1G56140*; *CERK1/AT3G14840*; *LYK4/AT2G23770*; *LYK5/AT2G33580*; *RBOHD/AT5G47910*.

AUTHOR CONTRIBUTIONS

MM-D performed research and generated data, designed some figures and reviewed the article. PF-C conceived, designed and performed research, generated data, designed some figures and wrote the article. PJS performed research on ECD purification and ITC assays, generated and analyzed the data, designed some figures and reviewed the article. GL performed research and generated data. MG-A designed and performed structural *in silico* analyses, designed some figures and wrote the article. DR performed research, generated data and designed some figures. IDH performed research and assembled *igp* mutant genomes. MAT and DJB performed research, generated reactive oxygen species production and designed some figures. VK performed research, generated data and reviewed the article. HM conceived and designed some experiments, analyzed data, designed some figures and revised the article. LFP conceived, designed and performed structural *in silico* analyses, designed some figures and wrote the article. JS conceived and designed ECD protein production and ITC binding experiments, analyzed the data, designed figures and wrote the article. AM conceived and designed the research, analyzed the data, designed figures and wrote the article.

CONFLICT OF INTEREST

All authors confirm that they have no conflicts of interest associated with this work.

ACKNOWLEDGEMENTS

We thank Dr Sonsoles Martín-Santamaria and Elena Gómez-Rubio (Centro de Investigaciones Biológicas Margarita Salas-CSIC, Spain) for their advice on deciphering the structure of the ECD LRR-MAL. We thank Dr Jose María Jiménez-Gomez and Dr René Toribio (Centro de Biotecnología y Genómica de Plantas (CBGP), Spain) for their kind advice on SNP identification and Western blotting, respectively. This work was supported by grant RTI2018-096975-B-I00 from the Spanish Ministry of Science, Innovation and Universities to AM and grant PID-2021-126006OB-100 from the Spanish Ministry of Science and Innovation to AM. This work has also been financially supported by the 'Severo Ochoa (SO) Programme for Centres of Excellence in R&D' from the Agencia

Estatal de Investigación (AEI) of Spain (grants SEV-2016-0672 (2017-2021) and CEX2020-000999-S (2022-2025) to the CBGP). In the frame of the SO program, HM and PF-C were supported with postdoctoral fellowships. MM-D, DJB and DR were recipients of PhD Fellows PRE2019-088120 and PRE2019-091276 (SEV-2016-0672) from AEI, and IND2017/BIO-7800 from Madrid Regional Government, respectively. Research in the lab of JS was financially supported by the University of Lausanne, the European Research Council (ERC) (grant agreement no. 716358) and the Swiss National Science Foundation (grant no. 310030_204526).

DATA AVAILABILITY STATEMENT

All relevant data can be found within the article and its supporting materials (Online data set; NCBI whole-genome sequence data set). Online data set include the genome assembly data for *igp1*^{AEQ}, *igp2*^{AEQ}, *igp3*^{AEQ}, *igp4* and Col-0^{AEQ} and can be retrieved from the NCBI Sequence Read Archive (SRA) under BioProject ID PRJNA864842 and Biosample accessions SAMN30087195, SAMN30087196, SAMN30087197, SAMN30087198 and SAMN30087199. Materials and data are available upon request to the corresponding authors.

SUPPORTING INFORMATION

Additional Supporting Information may be found in the online version of this article.

Figure S1. Forward genetic screening using Col-0^{AEQ} was used as a tool to discover PRRs and proteins involved in oligosaccharide perception and PTI activation.

Figure S2. Identification of additional *igp* (*igp5*–*igp9*) mutants impaired in MLG43 perception.

Figure S3. LRR-MAL-RK family in *Arabidopsis thaliana* includes additional members such as IGP4/AT1G56140, which is also required for MLG43 perception.

Figure S4. Developmental phenotypes of *igp* plants and LysM-PRR mutants.

Figure S5. Cytoplasmic calcium burst in response to CEL3 is impaired in *igp5*–*igp9* mutants.

Figure S6. Cross-elicitation during the refractory period of calcium burst triggered by MLG43 or CEL3.

Figure S7. ROS production triggered by flg22 and CHI6 in *igp1*–*igp4* mutants.

Figure S8. Activation of PTI hallmarks by MLG43, CEL3 and CHI6 in LysM-PRR mutants.

Figure S9. Phylogenetic analysis of LRR-MAL RKs in Arabidopsis and other plant species.

Figure S10. AlphaFold predictions for IGP1, IGP3 and IGP4 proteins.

Figure S11. Model structures of IGP1/CORK1, IGP3 and IGP4 proteins.

Figure S12. Purification of ECDs of IGP1/CORK1, IGP3 and IGP4 and ITC of IGP1/CORK1 binding of MLG43 and CEL3.

Table S1. Chi-square test statistics for *igp1*^{AEQ}–*igp3*^{AEQ} mutant segregation.

Table S2. Chromosomal localization of SNP mutations in *igp* mutants.

Table S3. Oligonucleotides used in this work.

REFERENCES

Andrews, S. (2010) FastQC: A Quality Control Tool for High Throughput Sequence Data.

Aziz, A., Gauthier, A., Bézier, A., Poinssot, B., Joubert, J.M., Pugin, A. *et al.* (2007) Elicitor and resistance-inducing activities of beta-1,4 cellodextrins in grapevine, comparison with beta-1,3 glucans and alpha-1,4 oligogalacturonides. *Journal of Experimental Botany*, **58**, 1463–1472.

Bacete, L., Mélida, H., Miedes, E. & Molina, A. (2018) Plant cell wall-mediated immunity: cell wall changes trigger disease resistance responses. *The Plant Journal*, **93**, 614–636.

Bacete, L., Schulz, J., Engelsdorf, T., Bartosova, Z., Vaahtera, L., Yan, G. *et al.* (2022) THESEUS1 modulates cell wall stiffness and abscisic acid production in Arabidopsis thaliana. *Proceedings of the National Academy of Sciences of the United States of America*, **119**, e2119258119.

Barghahn, S., Arnal, G., Jain, N., Petutschnig, E., Brumer, H. & Lipka, V. (2021) Mixed linkage β-1,3/1,4-Glucan oligosaccharides induce defense responses in Hordeum vulgare and Arabidopsis thaliana. *Frontiers in Plant Science*, **12**, 682439.

Bellande, K., Bono, J.J., Savelli, B., Jamet, E. & Canut, H. (2017) Plant lectins and lectin receptor-like kinases: how do they sense the outside? *International Journal of Molecular Sciences*, **18**, 1164.

Benedetti, M., Verrascina, I., Pontiggia, D., Locci, F., Mattei, B., De Lorenzo, G. *et al.* (2018) Four Arabidopsis berberine bridge enzyme-like proteins are specific oxidases that inactivate the elicitor-active oligogalacturonides. *The Plant Journal*, **94**, 260–273.

Bigeard, J., Colcombet, J. & Hirt, H. (2015) Signaling mechanisms in pattern-triggered immunity (PTI). *Molecular Plant*, **8**, 521–539.

Boutrot, F. & Zipfel, C. (2017) Function, discovery, and exploitation of plant pattern recognition receptors for broad-Spectrum disease resistance. *Annual Review of Phytopathology*, **55**, 257–286.

Brutus, A., Sicilia, F., Macone, A., Cervone, F. & De Lorenzo, G. (2010) A domain swap approach reveals a role of the plant wall-associated kinase 1 (WAK1) as a receptor of oligogalacturonides. *Proceedings of the National Academy of Sciences*, **107**, 9452–9457.

Burton, R.A. & Fincher, G.B. (2009) (1,3;1,4)-beta-D-glucans in cell walls of the poaceae, lower plants, and fungi: a tale of two linkages. *Molecular Plant*, **2**, 873–882.

Cao, Y., Liang, Y. & Tanaka, K. (2014) The kinase LYK5 is a major chitin receptor in Arabidopsis and forms a chitin-induced complex with related kinase CERK1. *eLife*, **3**, e03766.

Chaliha, C., Field, R.A. & Kalita, E. (2020) Glycans as Plant Defense Priming Agents Against Filamentous Pathogens. In: Mérillon, J.-M. & Ramawat, K.G. (Eds.) *Plant Defence: Biological Control*. Cham: Springer International Publishing, pp. 99–118.

Claverie, J., Balacey, S., Lemaître-Guillier, C., Brulé, D., Chiltz, A., Granet, L. *et al.* (2018) The Cell Wall-derived xyloglucan is a new DAMP triggering plant immunity in Vitis vinifera and Arabidopsis thaliana. *Frontiers in Plant Science*, **9**, 1725.

Cosgrove, D.J. (2022) Building an extensible cell wall. *Plant Physiology*, **189**, 1246–1277.

Cummings, R.D., Schnaar, R.L., Esko, J.D., Woods, R.J., Drickamer, K. & Taylor, M.E. (2022) Chapter 29. Principles of glycan recognition. In: Varki, A., Cummings, R.D. & Esko, J.D., ***et al.*** (Eds.) *Essentials of glycobiology*, 4th edition. Cold Spring Harbor, NY: Cold Spring Harbor Laboratory Press.

Danecek, P., Bonfield, J., Liddle, J., Marshall, J., Ohan, V., Pollard, M. *et al.* (2021) Twelve years of SAMtools and BCFtools. *GigaScience*, **10**, giab008.

del Hierro, I., Mélida, H., Broyart, C., Santiago, J. & Molina, A. (2021) Computational prediction method to decipher receptor–glycoligand interactions in plant immunity. *The Plant Journal*, **105**, 1710–1726.

Denoux, C., Galletti, R., Mammarella, N., Gopalan, S., Werck, D., De Lorenzo, G. *et al.* (2008) Activation of defense response pathways by OGs and Flg22 elicitors in Arabidopsis seedlings. *Molecular Plant*, **1**, 423–445.

Desaki, Y., Kouzai, Y., Ninomiya, Y., Iwase, R., Shimizu, Y., Seko, K. *et al.* (2018) OsCERK1 plays a crucial role in the lipopolysaccharide-induced immune response of rice. *The New Phytologist*, **217**, 1042–1049.

Dünser, K., Gupta, S., Herger, A., Feraru, M.I., Ringli, C. & Kleine-Vehn, J. (2019) Extracellular matrix sensing by FERONIA and leucine-rich repeat Extensins controls vacuolar expansion during cellular elongation in Arabidopsis thaliana. *The EMBO Journal*, **38**, e100353.

Felsenstein, J. (1985) Confidence limits on phylogenies: an approach using the bootstrap. *Evolution*, **39**, 783–791.

Fontaine, T., Simenel, C., Dubreucq, G., Adam, O., Delepierre, M., Lemoine, J. *et al.* (2000) Molecular organization of the alkali-insoluble fraction of aspergillus fumigatus cell wall. *The Journal of Biological Chemistry*, **275**, 27594–27607.

Franck, C., Westermann, J. & Boisson-Dernier, A. (2018) Plant Malectin-like receptor kinases: from Cell Wall integrity to immunity and beyond. *Annual Review of Plant Biology*, **69**, 301–328.

Fry, S.C., Nesselrode, B., Miller, J.G. & Mewburn, B.R. (2008) Mixed-linkage (1→3,1→4)-β-d-glucan is a major hemicellulose ofEquisetum(horsetail) cell walls. *The New Phytologist*, **179**, 104–115.

Gámez-Arjona, F.M., Vitale, S., Voxeur, A., Dora, S., Müller, S., Sancho-Andrés, G. *et al.* (2022) Impairment of the cellulose degradation machinery enhances Fusarium oxysporum virulence but limits its reproductive fitness. *Science. Advances*, **8**, eabl9734.

Gigli-Bisceglia, N., van Zelm, E., Huo, W., Lamers, J. & Testerink, C. (2022) Arabidopsis root responses to salinity depend on pectin modification and cell wall sensing. *Development*, **149**, dev200363.

Guo, H., Nolan, T.M., Song, G., Liu, S., Xie, Z., Chen, J. *et al.* (2018) FERONIA receptor kinase contributes to plant immunity by suppressing Jasmonic acid signaling in Arabidopsis thaliana. *Current Biology*, **28**, 3316–3324.e3316.

Gust, A.A., Biswas, R., Lenz, H.D., Rauhut, T., Ranf, S., Kemmerling, B. *et al.* (2007) Bacteria-derived peptidoglycans constitute pathogen-associated molecular patterns triggering innate immunity in Arabidopsis. *The Journal of Biological Chemistry*, **282**, 32338–32348.

Hashimoto, Y., Zhang, S., Zhang, S., Chen, Y.R. & Blissard, G.W. (2012) Correction: BTI-Tnao38, a new cell line derived from Trichoplusia ni, is permissive for AcMNPV infection and produces high levels of recombinant proteins. *BMC Biotechnology*, **12**, 12.

Huang, J., Rauscher, S., Nawrocki, G., Ran, T. & Feig, M. (2017) CHARMM36m: an improved force field for folded and intrinsically disordered proteins. *Nature Methods*, **14**, 71–73.

Humphrey, W., Dalke, A. & Schulten, K. (1996) VMD: visual molecular dynamics. *Journal of Molecular Graphics*, **14**(33–38), 27–38.

Jo, S., Kim, T. & Im, W. (2007) Automated builder and database of protein/membrane complexes for molecular dynamics simulations. *PLoS One*, **2**, e880.

Jo, S., Kim, T., Iyer, V.G. & Im, W. (2008) CHARMM-GUI: a web-based graphical user interface for CHARMM. *Journal of Computational Chemistry*, **29**, 1859–1865.

Johnson, J.M., Thürich, J., Petutschnig, E.K., Altschmied, L., Meichsner, D., Sherameti, I. *et al.* (2018) A poly(a) ribonuclease controls the Cellotriose-based interaction between Piriformospora indica and its host Arabidopsis. *Plant Physiology*, **176**, 2496–2514.

Jumper, J., Evans, R., Pritzel, A. & Green, T. (2021) Highly accurate protein structure prediction with AlphaFold. *Nature*, **596**, 583–589.

Jurrus, E., Engel, D., Star, K., Monson, K., Brandi, J., Felberg, L.E. *et al.* (2018) Improvements to the APBS biomolecular solvation software suite. *Protein Science*, **27**, 112–128.

Kaku, H., Nishizawa, Y., Ishii-Minami, N., Akimoto-Tomiyama, C., Dohmae, N., Takio, K. *et al.* (2006) Plant cells recognize chitin fragments for defense signaling through a plasma membrane receptor. *Proceedings of the National Academy of Sciences of the United States of America*, **103**, 11086–11091.

Klarzynski, O., Plesse, B., Joubert, J.M., Yvin, J.C., Kopp, M., Kloareg, B. *et al.* (2000) Linear beta-1,3 glucans are elicitors of defense responses in tobacco. *Plant Physiology*, **124**, 1027–1038.

Kloareg, B., Badis, Y., Cock, J.M. & Michel, G. (2021) Role and evolution of the extracellular matrix in the Acquisition of Complex Multicellularity in eukaryotes: a macroalgal perspective. *Genes*, **12**, 1059.

Knight, M.R., Campbell, A.K., Smith, S.M. & Trewavas, A.J. (1991) Transgenic plant aequorin reports the effects of touch and cold-shock and elicitors on cytoplasmic calcium. *Nature*, **352**, 524–526.

Kraemer, F.J., Lunde, C., Koch, M., Kuhn, B.M., Ruehl, C., Brown, P.J. *et al.* (2021) A mixed-linkage (1,3;1,4)-β-D-glucan specific hydrolase mediates dark-triggered degradation of this plant cell wall polysaccharide. *Plant Physiology*, **185**, 1559–1573.

Lee, H.K. & Goring, D.R. (2021) Two subgroups of receptor-like kinases promote early compatible pollen responses in the Arabidopsis thaliana pistil. *Journal of Experimental Botany*, **72**, 1198–1211.

Lemke, P., Jünemann, L. & Moerschbacher, B.M. (2022) Synergistic antimicrobial activities of chitosan mixtures and chitosan-copper combinations. *International Journal of Molecular Sciences*, **23**, 3345.

Li, H. (2013) Aligning sequence reads, clone sequences and assembly contigs with BWA-MEM. *arXiv*, 1303.3997v2.

Liu, S., Wang, J., Han, Z., Gong, X., Zhang, H. & Chai, J. (2016) Molecular mechanism for fungal Cell Wall recognition by Rice chitin receptor OsCEBiP. *Structure*, **24**, 1192–1200.

Liu, T., Liu, Z., Song, C., Hu, Y., Han, Z., She, J. *et al.* (2012) Chitin-induced dimerization activates a plant immune receptor. *Science*, **336**, 1160–1164.

Locci, F., Benedetti, M., Pontiggia, D., Citterico, M., Caprari, C., Mattei, B. *et al.* (2019) An Arabidopsis berberine bridge enzyme-like protein specifically oxidizes cellulose oligomers and plays a role in immunity. *The Plant Journal*, **98**, 540–554.

Luo, R., Schatz, M. & Salzberg, S. (2017) 16GT: a fast andsensitive variant caller using a 16-genotype probabilistic model. *GigaScience*, **6**(7), 1–4.

McClendon, C.L., Kornev, A.P., Gilson, M.K. & Taylor, S.S. (2014) Dynamic architecture of a protein kinase. *Proceedings of the National Academy of Sciences of the United States of America*, **111**, E4623–E4631.

Mélida, H., Bacete, L., Ruprecht, C., Rebaque, D., Del Hierro, I., López, G. *et al.* (2020) Arabinoxylan-oligosaccharides act as damage associated molecular patterns in plants regulating disease resistance. *Frontiers in Plant Science*, **11**, 1210.

Mélida, H., Sopeña-Torres, S., Bacete, L., Garrido-Arandia, M., Jordá, L., López, G. *et al.* (2018) Non-branched β-1,3-glucan oligosaccharides trigger immune responses in Arabidopsis. *The Plant Journal*, **93**, 34–49.

Mirdita, M. & Schütze, K. (2022) ColabFold: making protein folding accessible to all. *Nature Methods*, **19**, 679–682.

Mistry, J., Chuguransky, S., Williams, L., Qureshi, M., Salazar, G.A., Sonnhammer, E.L.L. *et al.* (2021) Pfam: the protein families database in 2021. *Nucleic Acids Research*, **49**, D412–d419.

Miya, A., Albert, P., Shinya, T., Desaki, Y., Ichimura, K., Shirasu, K. *et al.* (2007) CERK1, a Lys M receptor kinase, is essential for chitin elicitor signaling in Arabidopsis. *Proceedings of the National Academy of Sciences of the United States of America*, **104**, 19613–19618.

Morales, J., Kadota, Y., Zipfel, C., Molina, A. & Torres, M.A. (2016) The Arabidopsis NADPH oxidases Rboh D and Rboh F display differential expression patterns and contributions during plant immunity. *Journal of Experimental Botany*, **67**, 1663–1676.

Morgan, J.L., Strumillo, J. & Zimmer, J. (2013) Crystallographic snapshot of cellulose synthesis and membrane translocation. *Nature*, **493**, 181–186.

Moussu, S., Augustin, S., Roman, A.O., Broyart, C. & Santiago, J. (2018) Crystal structures of two tandem malectin-like receptor kinases involved in plant reproduction. *Acta crystallographica Section D, Structural Biology*, **74**, 671–680.

Nei, M. & Kumar, S. (2000) *Molecular evolution and phylogenetics*. USA: Oxford University Press.

Ngou, B.P.M., Ding, P. & Jones, J.D.G. (2022) Thirty years of resistance: zig-Zag through the plant immune system. *The Plant Cell*, **34**, 1447–1478.

Pérez-Mendoza, D., Rodríguez-Carvajal, M., Romero-Jiménez, L., Farias Gde, A., Lloret, J., Gallegos, M.T. *et al.* (2015) Novel mixed-linkage β-glucan activated by c-di-GMP in Sinorhizobium meliloti. *Proceedings of the National Academy of Sciences of the United States of America*, **112**, 757–765.

Pettersen, E.F., Goddard, T.D., Huang, C.C., Couch, G.S., Greenblatt, D.M., Meng, E.C. *et al.* (2004) UCSF chimera?A visualization system for exploratory research and analysis. *Journal of Computational Chemistry*, **25**, 1605–1612.

Pettolino, F., Sasaki, I., Turbic, A., Wilson, S.M., Bacic, A., Hrmova, M. *et al.* (2009) Hyphal cell walls from the plant pathogen Rhynchosporium secalis contain (1,3/1,6)-beta-D-glucans, galacto- and rhamnomannans, (1,3;1,4)-beta-D-glucans and chitin. *The FEBS Journal*, **276**, 3698–3709.

Pfaffl, M.W. (2001) A new mathematical model for relative quantification in real-time RT-PCR. *Nucleic Acids Research*, **29**, e45.

Phillips, J.C. & Hardy, D.J. (2020) Scalable molecular dynamics on CPU and GPU architectures with NAMD. *The Journal of Chemical Physics*, **153**, 44130.

Popper, Z.A. & Fry, S.C. (2003) Primary cell wall composition of bryophytes and charophytes. *Annals of Botany*, **91**, 1–12.

Putarjunan, A., Ruble, J. & Srivastava, A. (2019) Bipartite anchoring of SCREAM enforces stomatal initiation by coupling MAP kinases to SPEECHLESS. *Nature Plants*, **5**, 742–754.

Ranf, S., Eschen-Lippold, L., Pecher, P., Lee, J. & Scheel, D. (2011) Interplay between calcium signalling and early signalling elements during defence responses to microbe- or damage-associated molecular patterns. *The Plant Journal*, **68**, 100–113.

Ranf, S., Grimmer, J., Pöschl, Y., Pecher, P., Chinchilla, D., Scheel, D. *et al.* (2012) Defense-related calcium signaling mutants uncovered via a quantitative high-throughput screen in Arabidopsis thaliana. *Molecular Plant*, **5**, 115–130.

Rebaque, D., del Hierro, I., López, G., Bacete, L., Vilaplana, F., Dallabernardina, P. *et al.* (2021) Cell wall-derived mixed-linked β-1,3/1,4-glucans trigger immune responses and disease resistance in plants. *The Plant Journal*, **106**, 601–615.

Rzhetsky, A. & Nei, M. (1992) A simple method for estimating and testing minimum-evolution trees. *Molecular Biology and Evolution*, **9**, 945.

Saitou, N. & Nei, M. (1987) The neighbor-joining method: a new method for reconstructing phylogenetic trees. *Molecular Biology and Evolution*, **4**, 406–425.

Salmeán, A.A., Duffieux, D., Harholt, J., Qin, F., Michel, G., Czjzek, M. *et al.* (2017) Insoluble (1 → 3), (1 → 4)-β-D-glucan is a component of cell walls in brown algae (Phaeophyceae) and is masked by alginates in tissues. *Scientific Reports*, **7**, 2880.

Sandoval, P.J. & Santiago, J. (2020) In vitro analytical approaches to study plant ligand-receptor interactions. *Plant Physiology*, **182**, 1697–1712.

Schallus, T., Fehér, K., Sternberg, U., Rybin, V. & Muhle-Goll, C. (2010) Analysis of the specific interactions between the lectin domain of malectin and diglucosides. *Glycobiology*, **20**, 1010–1020.

Schallus, T., Jaeckh, C., Fehér, K., Palma, A.S., Liu, Y., Simpson, J.C. *et al.* (2008) Malectin: a novel carbohydrate-binding protein of the endoplasmic reticulum and a candidate player in the early steps of protein N-glycosylation. *Molecular Biology of the Cell*, **19**, 3404–3414.

Schrödinger, L.L.C. (2020) *The PyMOL molecular graphics system, version 2.5*. New York, NY: Schrödinger, LLC.

Shimizu, T., Nakano, T., Takamizawa, D., Desaki, Y., Ishii-Minami, N., Nishizawa, Y. *et al.* (2010) Two LysM receptor molecules, CEBiP and OsCERK1, cooperatively regulate chitin elicitor signaling in rice. *The Plant Journal*, **64**, 204–214.

Smakowska-Luzan, E., Mott, G.A., Parys, K., Stegmann, M., Howton, T.C., Layeghifard, M. *et al.* (2018) An extracellular network of Arabidopsis leucine-rich repeat receptor kinases. *Nature*, **553**, 342–346.

Soejima, Y., Lee, J., Nagata, Y., Mon, H., Iiyama, K., Kitano, H. *et al.* (2013) Comparison of signal peptides for efficient protein secretion in the baculovirus-silkworm system. *Open Life Sciences*, **8**, 1–7.

Sørensen, I., Pettolino, F.A., Wilson, S.M., Doblin, M.S., Johansen, B., Bacic, A. *et al.* (2008) Mixed-linkage (1→3),(1→4)-β-d-glucan is not unique to the Poales and is an abundant component of Equisetum arvense cell walls. *The Plant Journal*, **54**, 510–521.

Souza, C.A., Li, S. & Lin, A.Z. (2017) Cellulose-derived oligomers act as damage-associated molecular patterns and trigger defense-like responses. *Plant Physiology*, **173**, 2383–2398.

Tamura, K., Stecher, G., Peterson, D., Filipski, A. & Kumar, S. (2013) MEGA6: molecular evolutionary genetics analysis version 6.0. *Molecular Biology and Evolution*, **30**, 2725–2729.

Tang, D. & Wang, G. (2017) Receptor kinases in plant-pathogen interactions: more than pattern recognition. *The Plant Cell*, **29**, 618–637.

Tang, W., Lin, W., Zhou, X., Guo, J., Dang, X., Li, B. *et al.* (2022) Mechanotransduction via the pectin-FERONIA complex activates ROP6 GTPase signaling in Arabidopsis pavement cell morphogenesis. *Current Biology*, **32**, 508–517.e503.

Taylor, M., Drickamer, K., Imberty, A., van Kooyk, Y., Schnaar, R., Etzler, M. *et al.* (2022) Discovery and Classification of Glycan-Binding Proteins. In: Varki, A., Cummings, R.D., Esko, J.D. ***et al.*** (Eds.) *Discovery and Classification of Glycan-Binding Proteins*, editors edition. Cold Spring Harbor (NY): Cold Spring Harbor Laboratory Press.

Tseng, Y.-H., Scholz, S.S., Fliegmann, J., Krüger, T., Gandhi, A., Furch, A.C.U. *et al.* (2022) CORK1, a LRR-Malectin receptor kinase, is required for Cellooligomer-induced responses in Arabidopsis thaliana. *Cells*, **11**, 2960.

Tunyasuvunakool, K. & Adler, J. (2021) Highly accurate protein structure prediction for the human proteome. *Nature*, **596**, 590–596.

Versluys, M., Toksoy Öner, E. & Van den Ende, W. (2022) Fructan oligosaccharide priming alters apoplastic sugar dynamics and improves resistance against Botrytis cinerea in chicory. *Journal of Experimental Botany*, **73**, 4214–4235.

Voxeur, A., Habrylo, O., Guénin, S., Miart, F., Soulié, M.C., Rihouey, C. *et al.* (2019) Oligogalacturonide production upon Arabidopsis thaliana-Botrytis cinerea interaction. *Proceedings of the National Academy of Sciences of the United States of America*, **116**, 19743–19752.

Wan, J., He, M., Hou, Q., Zou, L., Yang, Y., Wei, Y. *et al.* (2021) Cell wall associated immunity in plants. *Stress Biology*, **1**, 3.

Wang, B., Qin, X., Wu, J., Deng, H., Li, Y., Yang, H. *et al.* (2016) Analysis of crystal structure of Arabidopsis MPK6 and generation of its mutants with higher activity. *Scientific Reports*, **6**, 25646.

Wanke, A., Rovenich, H., Schwanke, F., Velte, S., Becker, S., Hehemann, J.H. *et al.* (2020) Plant species-specific recognition of long and short β-1,3-linked glucans is mediated by different receptor systems. *The Plant Journal*, **102**, 1142–1156.

Waterhouse, A., Bertoni, M., Bienert, S., Studer, G., Tauriello, G., Gumienny, R. *et al.* (2018) SWISS-MODEL: homology modelling of protein structures and complexes. *Nucleic Acids Research*, **46**, W296–w303.

Willmann, R., Lajunen, H.M., Erbs, G., Newman, M.A., Kolb, D., Tsuda, K. *et al.* (2011) Arabidopsis lysin-motif proteins LYM1 LYM3 CERK1 mediate bacterial peptidoglycan sensing and immunity to bacterial infection. *Proceedings of the National Academy of Sciences of the United States of America*, **108**, 19824–19829.

Wong, J.E.M.M., Gysel, K., Birkefeldt, T.G., Vinther, M., Muszyński, A., Azadi, P. *et al.* (2020) Structural signatures in EPR3 define a unique class of plant carbohydrate receptors. *Nature Communications*, **11**, 3797.

Xiao, Y., Stegmann, M., Han, Z., DeFalco, T.A., Parys, K., Xu, L. *et al.* (2019) Mechanisms of RALF peptide perception by a heterotypic receptor complex. *Nature*, **572**, 270–274.

Yang, C., Liu, R., Pang, J., Ren, B., Zhou, H., Wang, G. *et al.* (2021a) Addendum: Poaceae-specific cell wall-derived oligosaccharides activate plant immunity via OsCERK1 during Magnaporthe oryzae infection in rice. *Nature Communications*, **12**, 3945.

Yang, C., Liu, R., Pang, J., Ren, B., Zhou, H., Wang, G. *et al.* (2021b) Poaceae-specific cell wall-derived oligosaccharides activate plant immunity via OsCERK1 during Magnaporthe oryzae infection in rice. *Nature Communications*, **12**, 2178.

Yang, C., Wang, E. & Liu, J. (2022) CERK1, more than a co-receptor in plant–microbe interactions. *New Phytologist*, **234**, 1606–1613.

Yang, H., Wang, D., Guo, L., Pan, H., Yvon, R., Garman, S. *et al.* (2021) Malectin/Malectin-like domain-containing proteins: a repertoire of cell surface molecules with broad functional potential. *The Cell Surface*, **7**, 100056.

Zang, H., Xie, S., Zhu, B., Yang, X., Gu, C., Hu, B. *et al.* (2019) Mannan oligosaccharides trigger multiple defence responses in rice and tobacco as a novel danger-associated molecular pattern. *Molecular Plant Pathology*, **20**, 1067–1079.

Zarattini, M., Corso, M., Kadowaki, M.A., Monclaro, A., Magri, S., Milanese, I. *et al.* (2021) LPMO-oxidized cellulose oligosaccharides evoke immunity in Arabidopsis conferring resistance towards necrotrophic fungus B. cinerea. *Communications Biology*, **4**, 727.

Zhang, Y. & Skolnick, J. (2005) TM-align: a protein structure alignment algorithm based on the TM-score. *Nucleic Acids Research*, **33**, 2302–2309.